

ELECTRICALLY TUNABLE PLASMON INDUCED TRANSPARENCY IN HYBRID METAL-GRAPHENE STRUCTURES

A THESIS SUBMITTED TO
THE GRADUATE SCHOOL OF ENGINEERING AND SCIENCE
OF BILKENT UNIVERSITY
IN PARTIAL FULFILLMENT OF THE REQUIREMENTS FOR
THE DEGREE OF
MASTER OF SCIENCE
IN
ELECTRICAL AND ELECTRONICS ENGINEERING

By
Mohsin Habib
June 2018

ELECTRICALLY TUNABLE PLASMON INDUCED TRANSPARENCY IN HYBRID METAL-GRAPHENE STRUCTURES

By Mohsin Habib

June 2018

We certify that we have read this thesis and that in our opinion it is fully adequate, in scope and in quality, as a thesis for the degree of Master of Science.

Ekmel Özbay(Advisor)

Hümeyra Çağlayan(Co-Advisor)

Vakur B. Erturk

Hamza Kurt

Approved for the Graduate School of Engineering and Science:

Ezhan Kardeşan
Director of the Graduate School

ABSTRACT

ELECTRICALLY TUNABLE PLASMON INDUCED TRANSPARENCY IN HYBRID METAL-GRAPHENE STRUCTURES

Mohsin Habib

M.S. in Electrical and Electronics Engineering

Advisor: Ekmel Özbay

Co-Advisor: Hümeyra Çağlayan

June 2018

Hybrid metal-graphene structures offer design flexibility to manipulate and control light efficiently. These structures can be used to generate tunable plasmon induced transparency (PIT) in transmission and reflection mode. PIT is plasmonic analogue of electromagnetically induced transparency (EIT). PIT and reflection type PIT (RPIT) devices have been investigated experimentally but they are not tunable, and the numerical investigations of the tunable designs were limited to simulations. A hybrid metal-graphene design is used to overcome these challenges in this thesis. Tunable PIT and RPIT devices can be used for tunable enhanced biosensing and switchable systems. PIT-effect has been numerically investigated and experimentally realized in two devices with different dimensions. Numerical simulations were performed using Finite Difference Time-Domain (FDTD) method. The design is based on two parallel gold (Au) strips on top of the graphene layer. PIT-effect has been achieved by weak hybridization of two bright modes of these Au strips. The PIT-effect is tuned by changing the Fermi energy (E_f) of graphene. Top gating method is used to achieve high tunability in the experiments. Total shift of 263 nm is obtained in the PIT window by applying the gate voltage up to 3 V. The spectral contrast ratio of the devices is up to 82%. In addition, tunable RPIT effect is achieved using the same metal-graphene structure. I have numerically investigated the four layers design and experimentally realized tunable RPIT. The response of this device is also tuned using top gating method. The tunability of 220.8 nm is observed in RPIT peak for 3 V.

Keywords: Plasmon induced transparency, hybrid metal-graphene, and electrically tunable.

ÖZET

HİBRİT METAL-GRAFEN YAPILARINDA ELEKTRİKLE DEĞİŞTİRİLEBİLEN PLAZMONLA UYARILMIŞ GEÇİRGENLİK

Mohsin Habib

Elektrik ve Elektronik Mühendisliği, Yüksek Lisans

Tez Danışmanı: Ekmel Özbay

İkinci Tez Danışmanı: Hümeysra Çağlayan

Haziran 2018

Hibrid metal-grafen yapıları, ışığı etkili bir şekilde manipüle etmek ve kontrol etmek için tasarım esnekliği sağlar. Bu yapılar, iletim (transmission) ve yansıma (reflection) modlarında ayarlanabilen plazmonla uyarılmış geçirgenlik (PIT) üretmek için kullanılabilir. PIT elektromanyetik olarak indüklenen geçirgenliğin (EIT) bir plazmonik analogudur. PIT ve Yansıma Tipi PIT (RPIT) aygıtlar, deneysel olarak farklı gruplar tarafından incelenmiştir fakat bunlar ayarlanamaz ve bunların ayarlanabilir tasarımların sayısal analizleri simülasyonlar ile sınırlanmıştır. Bu tezde bu zorlukların üstesinden gelebilmek için bir hibrit metal-grafen tasarımı kullanılmıştır. PIT-etkisi sayısal olarak incelenmiş ve farklı boyutlardaki iki aygıtta deneysel olarak gerçekleştirilmiştir. Sayısal simülasyonlar Zamanda Sonlu Farklar (FDTD) yöntemi kullanılarak gerçekleştirilmiştir. Tasarım, grafen tabakasının üzerinde bulunan iki paralel altın şeridine dayanmaktadır. PIT-etkisi bu altın şerittin, iki parlak modunun zayıf hibridizasyonu ile başarılmıştır. PIT-etkisi grafenin Fermi enerjisinin (E_f) değişimi ile ayarlanır. Üstten kapılama metodu, deneylerde yüksek ayarlanabilirliğe ulaşmak için kullanılmıştır. 3V'a kadar Gate (kapı) voltajı uygulanarak PIT penceresinde toplam 263 nm kayma elde edilmiştir. Bu cihazların spectral kontrast (izgesel karşıtlık) oranı % 82'ye kadardır. Ek olarak, ayarlanabilir RPIT etkisi aynı metal-grafen yapısı kullanarak elde edilmiştir. Ayarlanabilir RPIT dört katmanlı tasarımı, sayısal olarak araştırıldı ve deneysel olarak gerçekleştirildi. Bu aygıtın tepkisi de üstten kapılama yöntemi kullanılarak ayarlanmaktadır. 220.8 nm' lik bir ayarlanabilirliği RPIT zirvesinde 3 V ile gözlemlenmiştir.

Anahtar sözcükler: Plazmon uyarılmış geçirgenlik, ve hibrit metal-grafen, elektriksel olarak ayarlanabilir.

Acknowledgement

I would like to express my deepest gratitude to the Professor Ekmel Özbay for his advice and support during my master's at Bilkent University. Without his support and guidance, it would have been impossible to achieve all the results which are presented in my thesis. He is very kind and humble person equipped with deep knowledge and ideas. With proper guidance and available facilities at Nanoteknoloji Araştırma Merkezi (NANOTAM) he provides enough resources and freedom to explore new ideas. I would like to acknowledge his leadership qualities and making NANOTAM a complete research center for studying nanotechnology and related fields.

I have no words to express my gratitude to the Professor Hümeyra Çağlayan, she has been mentor since the first day I have joined NANOTAM. She has always guided me in all kind of research related problems. She has taught me to work with Lumerical software, fabrication and characterization of my device in a very easy and efficient way. All the discussions during the meetings with her were very productive and beneficial for me. I am very thankful for her insightful comments that greatly improved my thesis. She is currently a professor at TUT, Finland and has invited me to do my Ph.D under her supervision in Metaplasmonics group.

I am thankful to Professor Vakur B. Erturk and Professor Hamza Kurt for reviewing my thesis. Their comments and suggestions were beneficial to improve the quality of my thesis.

I am thankful to Dr. Alireza Rahimi Rashed, who was like a brother to me. He trained me nano-fabrication and characterization of my devices. I have discussed my ideas with him and his comments were always beneficial for me.

I would like to appreciate the support of all the people from NANOTAM and especially Murat Gokbayrak for his help to realize my ideas. I always enjoyed sharing the office with Majid Alizadeh, Salahuddin Zafar (Bhai) and Yiğit

Demirağ. As department secretary, Mürüvet Parlakay was always kind and helpful in administrative affairs, I really appreciate her efforts.

Turkey became my second home by having wonderful people around me since the first day I arrived at Bilkent University. I am really thankful for the support of Muhammad Anjum Qureshi (Bhai), Ali Hassan Mirza, Muhammad Hamza Humayun, Muhammad Umar B. Niazi and rest of the grad students from Pakistan.

I will always be thankful to my parent; they have supported me throughout my academic career. They inspired me with their hard work. I would like to thank my life partner (Rabia) for the support and encouragement to pursue my master's studies in Turkey. I was lucky to have supportive brother and sisters. A video calls with my adorable nieces (Barzaah, Faliha, and Mehmoona) were always refreshing.

My studies at Bilkent University were funded by Higher Education Commission, Pakistan.

Contents

1	Introduction	1
1.1	Organization of the thesis	2
2	Theory	3
2.1	Introduction to graphene	3
2.1.1	Band diagram of graphene	4
2.1.2	Optical response of graphene	5
2.2	Plasmon induced transparency	7
2.2.1	Tunable plasmon induced transparency	10
2.2.2	Hybrid design for tunable plasmon induced transparency	12
3	Electrically tunable Plasmon Induced Transparency	14
3.1	Introduction	14
3.2	Design and Simulations	16
3.3	Fabrication Process	18

<i>CONTENTS</i>	ix
3.3.1 Graphene transfer	18
3.4 E-beam lithography	19
3.4.1 E-beam evaporation	20
3.4.2 Top gating	21
3.4.3 Photolithography	22
3.5 Characterization	23
3.5.1 Characterization of graphene	23
3.5.2 Characterization of the fabricated samples	24
3.6 Results	27
3.6.1 Mode profile	31
3.6.2 Performance	32
3.7 Conclusion	33
4 Reflection type Tunable Plasmon Induced Transparency	34
4.1 Introduction	34
4.2 Design and Simulations	35
4.3 Fabrication	37
4.4 Results	38
4.4.1 Mode profile	40
4.4.2 Performance	40

<i>CONTENTS</i>	x
4.5 Conclusion	41
5 Conclusion and Outlook	42
A Publications	52

List of Figures

2.1	Left: electronic structure of sp^2 hybridized six neighboring carbon atoms. Right: zoom-in picture of Dirac point of graphene [37]. . .	4
2.2	Frequency dependent complex surface conductivity for graphene (a) real and (b) imaginary parts. [27].	6
2.3	Schematic of nanostructures for PIT-effect. (a) Unit cell for dark-bright modes for PIT [52]. (b) Two layers metamaterial for PIT-effect [20]. (c) Schematic of nanospheres for PIT [17]. (d) Schematic of a unit cell for PIT effect by mirror images of ring resonators [53].	9
2.4	Schematic for tunable PIT-effect. (a) Graphene ring and graphene strip [54]. (b) Top view of the unit cell for cascaded π -shaped PIT design with the dimensions [55]. (c) Schematic of two parallel strips of graphene for tunable PIT-effect with dimensions [57]. . .	11
2.5	Schematic of hybrid graphene-metal metamaterial for tunable PIT [27].	12

3.1	Unit cell of PIT structures, two Au strips (golden) with different lengths on graphene (grey). Both the devices have the same periodicity of $5.2 \mu\text{m}$ in x -axis and y -axis. (a) The lengths of strips are $3.2 \mu\text{m}$ and $2.4 \mu\text{m}$ for the first device. (b) The lengths of strips are $3.4 \mu\text{m}$ and $2.6 \mu\text{m}$ for the second device.	15
3.2	Schematic of simulation setup. (a) 3D view of PIT device, BaF_2 is used as transparent substrate with a graphene layer and Au strips on top of graphene. (b) Complete simulation setup of PIT device, plane wave source for exciting the structure, two monitors for E-field and transmission measurements.	17
3.3	Microscope image of graphene transfer (a) Image from 5X eyepiece showing the corner of graphene layer on top of Si substrate. (b) Image from 50X eyepiece showing surface of graphene.	19
3.4	Schematic of E-beam evaporation setup. Electrons generated from ion source are accelerated towards source crucible. The materials are evaporated and deposit onto patterned sample, attached to sample holder [62].	21
3.5	Schematic of top gating of PIT device. Two BaF_2 substrates are used. The first one with Au strips on graphene, which is connected to the source by conductive tape. The second one with a window for FTIR measurements and coated with Ti/Au, which is connected to the second terminal of the source. Ionic liquid (transparent area) is injected between these two substrates.	22
3.6	Raman signal of a graphene layer on Si sample using wet transfer method.	24
3.7	SEM images of PIT device. (a) Image for multiple unit cells. (b) SEM image of first device with shorter lengths of Au strips. (c) SEM image of second device with longer lengths of Au strips.	25

3.8	AFM measurement of PIT device. (a) 3D topography of a sample surface. (b) Height measurement of the sample, height of two strips is 70 nm.	26
3.9	Comparison of PIT-effect for the device with shorter dimensions (black) and the device with longer dimensions (red).	28
3.10	Simulated and FTIR measurement of PIT structures. (a) Simulated results of first device (3.2 μm and 2.4 μm) for different E_f . (b) Normalized transmission for first device (shorter dimensions) at -0.6 V, 0.9 V and 2.4 V.	29
3.11	Simulated and FTIR measurement of PIT structures. (a) Simulated results of second device (3.4 μm and 2.6 μm) for different E_f . (b) Normalized transmission for second device (longer dimensions) at -0.6 V, 0.9 V and 2.4 V.	30
3.12	E-field magnitude for first device (shorter dimensions) at 0.5 eV (a) E-field magnitude at 7.746 μm . (b) E-field magnitude at 8.217 μm (c) E-field magnitude at 9.056 μm	31
3.13	Total shift of transmission peak for device with first device (black) and second device (red).	32
4.1	Unit cell of PIT structure. Two Au strips (golden) with lengths of L1(0.8 μm), L2(1 μm), W (200 nm) is width and D (200 nm) is distance between two strips. Px (1.5 μm) and Py (1 μm) show periodicity of unit cell.	35
4.2	Schematic of simulation setup. (a) 3D view of RPIT device, Si is used as substrate with an Al and Al ₂ O ₃ for reflective and dielectric layers. Au strips on top of graphene. (b) Complete simulation setup with a RPIT device, plane wave source for exciting the structure, two monitors for E-field and reflection measurements.	36

4.3	SEM images of RPIT structures.	37
4.4	Simulated and FTIR measurement of RPIT structures. (a) Simulated results for different E_f . (b) Normalized transmission at -0.6 V, 0.9 V and 2.4 V.	39
4.5	E-field magnitude at 0.5 eV (a) E-field magnitude at 3.65 μm . (b) E-field magnitude at 4.420 μm (c) E-field magnitude at 3.87 μm .	40

Chapter 1

Introduction

The electromagnetically induced transparency (EIT) effect has been studied for several years due to the great potential in slow light applications [1, 2, 3], quantum information processing [4], optical switching [5], optical storage [6, 7], biosensing [8, 9, 10], optical modulation, and nonlinear enhancement in photonics [11]. The EIT-effect can be realized by a three-level atomic system in which destructive interference of the two excitation pathways result in a narrow transparency window [12, 13, 14, 15].

Recently, the plasmon induced transparency (PIT), a novel effect analogous to the EIT-effect has been investigated. The PIT has been observed in the variety of platforms, such as metallic nanoparticles [16, 17], metamaterial structures [18, 19, 20, 21, 22, 23], plasmonic coupled nanocavities [24], hybrid plasmon waveguide systems [25], and integrated photonic structures [26]. Metamaterials are known as a powerful tool to control and manipulate the interaction of light with materials. Therefore, the PIT designs based on metamaterial structures are the most promising as they can be engineered for the desired optical response. Moreover, these designs can be tunable by the variety of tuning mechanisms such as electrical, optical and thermal [23]. By integrating metamaterials that produce PIT-effect with an actively tunable material such as graphene [27] can offer promising applications, such as tunable enhanced sensing and switchable systems.

In this thesis, I have numerically investigated and experimentally realized electrically tunable PIT-effect in hybrid metal-graphene structures. The hybrid metamaterial structure is composed of two parallel gold (Au) strips on top of the graphene layer. The PIT-effect is generated by the two strips with different lengths. This effect is tuned electrically by changing the Fermi level (E_f) of graphene using top gating method [28]. Moreover, I have achieved tunable PIT-effect in the reflection mode with a similar hybrid device.

1.1 Organization of the thesis

The organization of my thesis is summarized as follow: in the second chapter, I studied the theoretical background of electrical, and optical properties for graphene. The unique band structure of graphene and its application in tunable plasmonics. I have discussed the state-of-the-art designs for PIT-effect and tunable PIT-effect. I have highlighted the challenges associated with the design presented in the literature for tunable PIT-effect. Following up with the motivation of designing hybrid metal-graphene structures for electrically tunable PIT-effect.

In the third chapter, I have presented the numerical investigation of two gold strips on graphene. The fabrication details of graphene transfer, E-beam lithography, E-beam evaporation and characterization of the devices. I have discussed the top gating method which has been used for tuning the PIT-effect and the results of normalized transmission and electric field.

In the fourth chapter, I have investigated similar structures but in reflection mode for different range of wavelength. I have also tuned electrically the PIT-effect in the reflection mode (RPIT).

In the last chapter, the thesis provides conclusion and outlook of the tunable PIT and RPIT work.

Chapter 2

Theory

2.1 Introduction to graphene

Graphene is a single atomic layer thick material, also known to be the first ever a 2D material, in which carbon atoms form a honeycomb lattice [29]. Graphene was discovered back in 2004 by Novoselov *et al.* For this groundbreaking discovery, they were awarded a Nobel Prize in Physics [30]. Graphene is a building block of all graphitic allotropes of carbon. Before the discovery of graphene, it remained unsettled that free-standing atomic layer thick material could exist or not. It was believed that materials below the thickness of dozen atomic layers are thermally unstable. However, after 2004, a completely new research area emerged on 2D materials because these material are not only stable at few atomic layer thickness but they have high crystal quality [31].

Graphene has remarkable electrical, mechanical, and optical properties. Among these ballistic transport of charge carriers [32], tunable intraband transition [33, 34] and quantum Hall effect [35] are the most exotic properties. Moreover, Young's modulus of monolayer graphene was reported to be 1.0 TPa, confirming that graphene is the strongest material [36].

2.1.1 Band diagram of graphene

Graphene is considered to be a semi-metal since the conduction and the valence band intersect at a single Dirac point. The Graphene's crystal structure has two sublattices. The quantum mechanical hopping among these sublattices will create two energy bands. The intersection of these bands near the edges of Brillouin zone results in a conical shaped energy band, shown in Figure 2.1 [37]. This will lead to a linear dispersion relation. Due to this linear dispersion quasiparticles of graphene behave like massless relativistic particles.

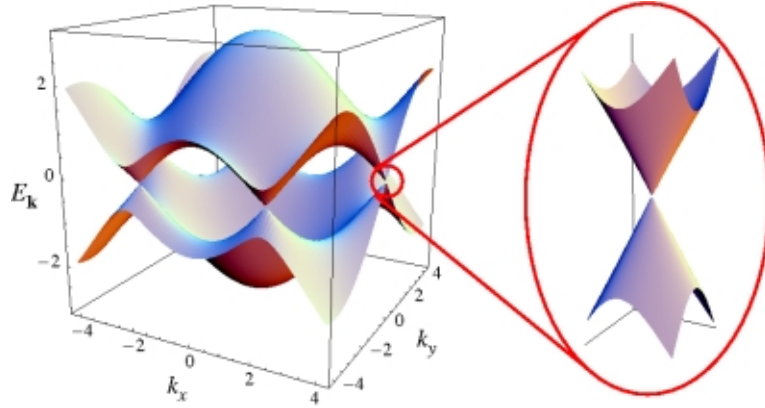


Figure 2.1: Left: electronic structure of sp^2 hybridized six neighboring carbon atoms. Right: zoom-in picture of Dirac point of graphene [37].

For intrinsic graphene E_f is exactly at the Dirac point. By changing the charge density (n), E_f of graphene can be tuned and is described as:

$$E_f = \hbar\nu_f\sqrt{\pi n} \quad (2.1)$$

where \hbar is the reduced Planck's constant (6.62×10^{-34} J-s) and ν_f is Fermi velocity (1.1×10^8 cm s^{-1}) [38].

2.1.2 Optical response of graphene

Optical properties of the graphene can be explained by Pauli Blocking [39] principal, as graphene forms a conical band diagram, shown in Figure 2.1. Near the intersection of the cones, graphene has a low density of states which allows significant changes in the E_f with variation doping. Therefore, optical properties of graphene can be tuned by doping. Two types of band transitions are possible depending upon the energy of the incident photon. If the energy of photon is less than $2E_f$ intra-band transition is dominant, because of the lack of available states for this energy level at that momentum. On the other hand, if the photon energy is higher than $2E_f$ inter-band transition is dominant [40, 41]. The interplay of these transitions establishes the optical response of graphene.

The surface conductivity of graphene can be modeled as an infinitesimally thin an isotropic surface with conductive from both the sides. Intra-band transition is presented in equation 2.2 and inter-band transitions in equation 2.3 [42]:

$$\sigma_{intar}(\omega, \mu_c, \Gamma, T) = -j \frac{e^2 k_B T}{\pi \hbar^2 (\omega - 2j\Gamma)} \left[\frac{\mu_c}{k_B T} + 2 \ln \left(e^{\frac{-\mu_c}{k_B T}} + 1 \right) \right] \quad (2.2)$$

$$\sigma_{inter}(\omega, \mu_c, \Gamma, T) = -j \frac{e^2}{4\pi \hbar} \ln \left[\frac{2|\mu_c| - (\omega - 2j\Gamma)\hbar}{2|\mu_c| + (\omega - 2j\Gamma)\hbar} \right] \quad (2.3)$$

where e is the electron charge (1.60×10^{-19}) and k_B is the Boltzmann's constant ($1.38 \times 10^{-23} \text{ m}^2 \text{ Kg s}^{-2} \text{ K}^{-1}$). Other parameters include the temperature (T), the scattering rate Γ , the angular frequency (ω_c), and the chemical potential (μ_c) which can be changed in numerical investigations.

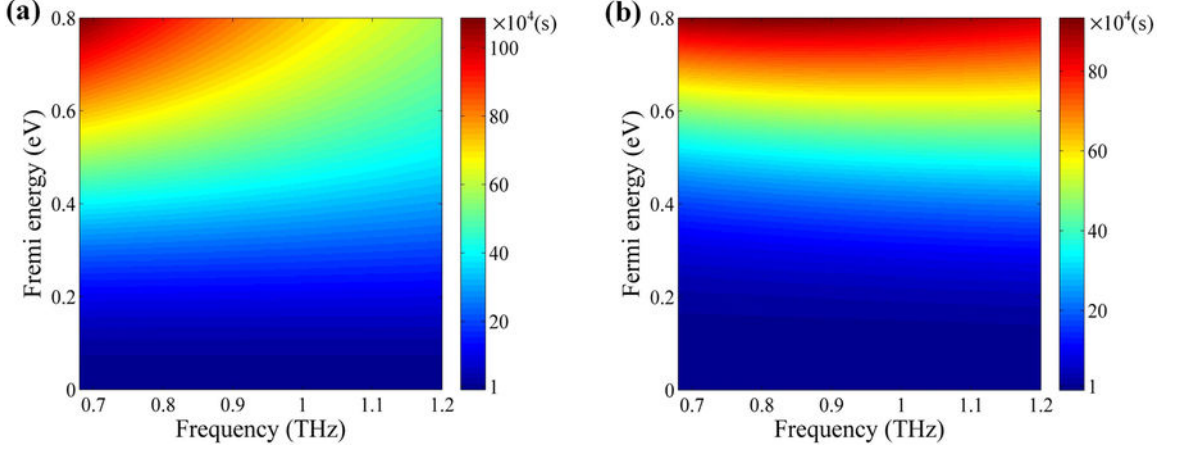


Figure 2.2: Frequency dependent complex surface conductivity for graphene (a) real and (b) imaginary parts. [27].

Figure 2.2 shows the real and imaginary part of overall surface conductivity as the function of frequency and corresponding E_f [27]. Surface conductivity is increased by increasing the E_f of graphene. Relaxation time ($\tau = -1/(2\Gamma)$) is dependent on the quality of graphene layer. It is the function of carrier mobility (μ), μ_c and ν_f :

$$\tau = \frac{\mu\mu_c}{ev_f} \quad (2.4)$$

The high relaxation time reduces the transmission attenuation. However, the quality of graphene during the transfer process limit the relaxation time to few fs.

The explicit dependence of the intra-band conductivity (2.2) on E_f of graphene implies that optical response of graphene is controllable in the mid infrared (MIR) region. Therefore, it is possible to obtain tunable absorption in MIR regime [41, 43]. The optical response can be tuned by several methods. It can be controlled by chemical, optical and electrostatic doping [44]. Among these electrostatic doping is widely used for optoelectronics applications [45, 46]. It is effective and can tune the response actively.

Overall at optical frequencies, graphene has three major advantages. First, being a 2D material, it enables device miniaturization down to the atomic length

scale. Second, the doping level in monolayer graphene is highly tunable by applying a voltage to an electrical gate. Third, graphene exhibits an optical response ranging from terahertz to optical frequencies, allowing for ultra-broadband operation. In particular, broadband optical modulators have been demonstrated [33]. The optical response of graphene originates from two different processes: intra-band transitions in the conduction or valence band give rise to a Drude-like response similar to noble metals, and inter-band transitions which are Pauli blocked for frequencies below twice the Fermi energy give rise to a universal, flat absorption spectrum. The Drude response is typically observed for frequencies up to the far-infrared, whereas the flat absorption of 2.3% is observed at optical frequencies [47].

2.2 Plasmon induced transparency

The interaction of light with the electrons of metal that can move freely is defined as plasmonics. If metallic nanostructures are smaller than the size of the incident wavelength of light will result in collective oscillation of these electrons. This phenomenon is known as localized surface plasmon resonance (LSPR). The wavelength and intensity of these resonances are dependent on the material, shape, and size of nanostructures [48]. Different plasmon modes can interact by the near-field coupling. The type of coupling can be explained by plasmon hybridization theory [49].

The plasmonic mode can be either radiative (bright mode) or subradiant (dark mode) [50]. If the incident light couple's directly then it will produce bright modes which are spectrally broadened due to radiative damping. On the other hand, if the incident light is not coupled directly, it will generate dark modes which are weakly damped and spectrally narrow [51]. PIT has been realized by either destructive interference of dark-bright modes or detuning of two bright modes.

The PIT-effect was demonstrated by single strip and two parallel strips, serving

as bright and dark modes, respectively, shown in Figure 2.3 (a) [52]. Experimental demonstration of the PIT-effect was presented by Liu *et al.* in an optical metamaterial in 2009. The structures consist of the two layers, a gold (Au) bar was stacked above two strips of Au wire, shown in Figure 2.3 (b) [20]. The PIT-effect was controlled by lateral displacement of the bar above two wires. Similarly, bi-layered metamaterials were used to observe PIT effect in Reference [18].

The PIT-effect has been numerically investigated in visible regime by Au spheres with indium tin oxide (ITO) layer, shown in Figure 2.3 (c) [17]. The PIT phenomenon emerges when Au spheres strongly couple with incident light and exhibit bright mode. The dark mode is provided by ITO waveguide.

The PIT-effect was presented in different systems of ring resonators [19, 22, 53]. Among these designs, mirror-like symmetrical metamaterials were numerically investigated and experimentally realized [53]. In this work, two ring resonators serve as the bright mode and other two serves as the dark mode, shown in Figure 2.3 (d) [53].

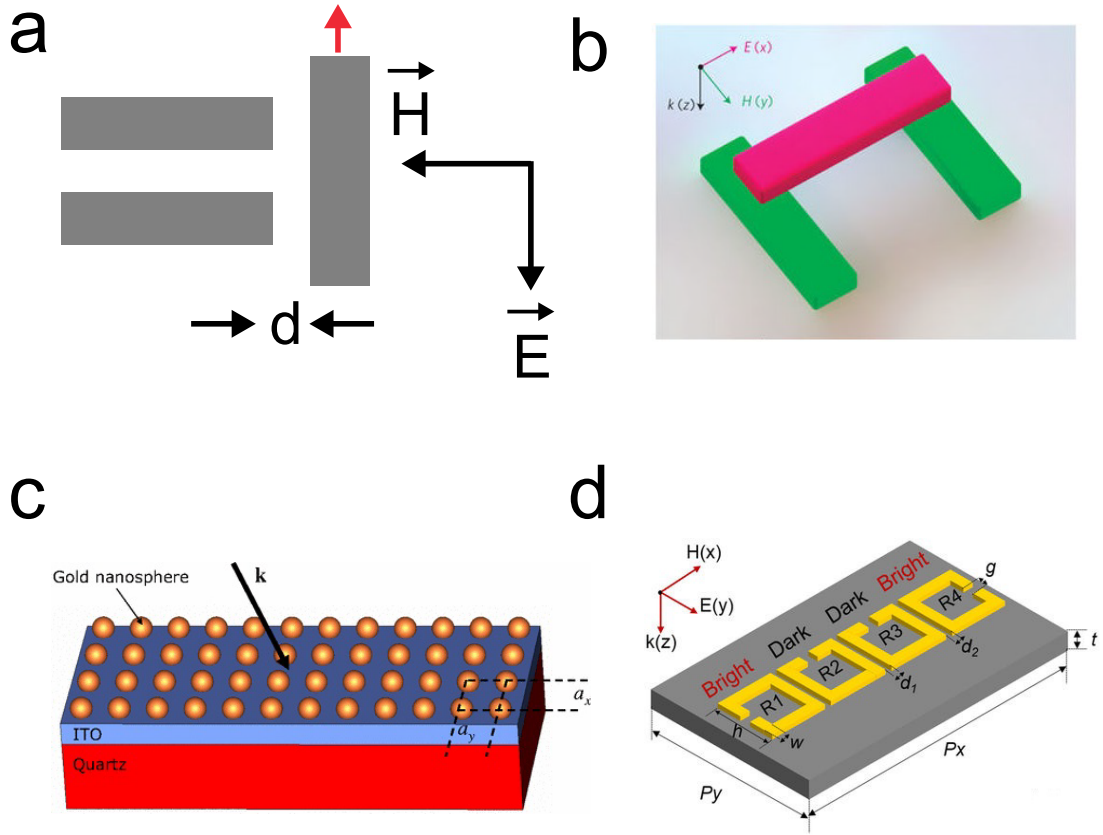


Figure 2.3: Schematic of nanostructures for PIT-effect. (a) Unit cell for dark-bright modes for PIT [52]. (b) Two layers metamaterial for PIT-effect [20]. (c) Schematic of nanospheres for PIT [17]. (d) Schematic of a unit cell for PIT effect by mirror images of ring resonators [53].

However, all of these designs are based on metals which are limited by inherent propagation loss and it is hard to control the permittivity of the metals. This limits the design with low modulation range. For tuning mostly geometrical parameters of designs are changed and require refabrication. The active control of the PIT-effect is limited in these designs.

2.2.1 Tunable plasmon induced transparency

Recently, tunable PIT-effect has been numerically investigated by several groups. These designs are based on graphene metamaterials which can be tuned by altering the E_f of graphene as discussed in section 2.2. Zhang *et al.* presented graphene-based metamaterial, which consists of a graphene strip and a ring for terahertz PIT-effect. In this work, both the ring and the strip are serving as bright modes, shown in Figure 2.4 (a) [54]. The weak hybridization of these modes lead to the PIT-effect that was controlled by adjusting the geometric parameters. Moreover, the resonance of both the modes can be tailored dynamically using tunable E_f of graphene. The PIT window was shifted to 0.21 THz in total.

Similarly, in another numerical investigation of cascaded π -shaped graphene nanostructures PIT-effect is presented. They studied the transmission properties of the design, shown in Figure 2.4 (b) [55]. They were able to tune the response electrically using graphene up to 17 THz and propose their design for bio sensing and photonics applications.

Some groups have also investigated designs based on parallel strips of graphene [56, 57]. In their designs, each strip serves as bright mode and their coupling results in PIT-effect, shown in Figure 2.4 (c). Total shift of 0.2 THz is reported in their work. The weak hybridization of these modes produces PIT-effect, which is controlled by simply adjusting the lengths, width, and distance between the strips. Their designs are simple and electrically tunable.

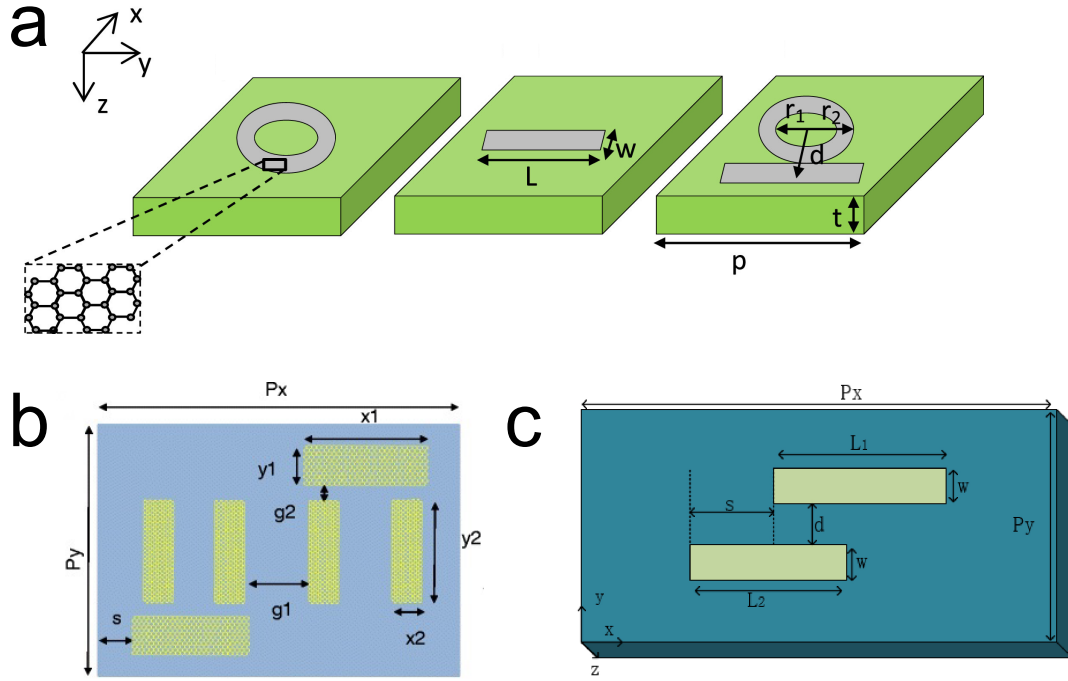


Figure 2.4: Schematic for tunable PIT-effect. (a) Graphene ring and graphene strip [54]. (b) Top view of the unit cell for cascaded π -shaped PIT design with the dimensions [55]. (c) Schematic of two parallel strips of graphene for tunable PIT-effect with dimensions [57].

Other designs include two asymmetric slot structures of graphene [58], Fabry-Perot type resonators [59] and graphene on top of the silicon-air grating structure [60] for demonstrating PIT-effect. However, the successful realization of all these tunable PIT designs has not been reported due to the fabrication and gating limitations in experiments. Graphene based structures require high quality graphene layer on the desired substrate without defects/cracks which develop during the transfer procedure. These cracks are comparable with the proposed structures and can alter the response significantly. Therefore, in this thesis a hybrid metal-graphene design is proposed, to overcome the problems associated with graphene structures.

2.2.2 Hybrid design for tunable plasmon induced transparency

Graphene has been recognized as a new class of materials with unique plasmonic properties that can be tuned by electrostatic doping. However, patterning graphene structures are limited by the transferred quality of the graphene. Yan *et al.* came up with a novel idea of a hybrid metal-graphene based metamaterial design for tunable PIT-effect. They have numerically investigated a strip without the graphene layer and a ring with the graphene layer at the bottom, shown in Figure 2.5 [27]. In their design, they were able to tune the amplitude of PIT-effect using graphene.

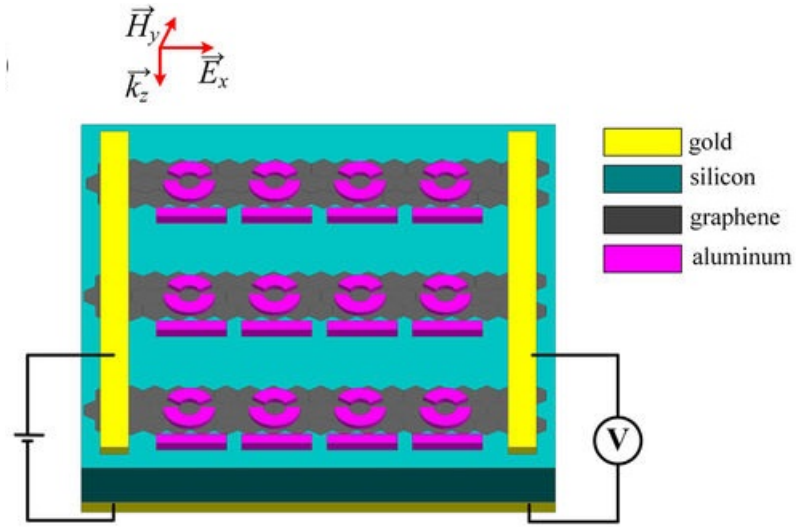


Figure 2.5: Schematic of hybrid graphene-metal metamaterial for tunable PIT [27].

Recently, Liu has presented a hybrid metamaterial for tunable PIT-effect. In this work, a monolayer of graphene was placed on top of the metamaterial for numerical investigation. The resonance strength of metamaterial was tailored by changing the E_f of the graphene. A split ring resonator is enclosed inside closed ring resonator [23] in their structure.

In hybrid metal-graphene designs PIT-effect is generated using metallic structures. The response is not controlled by the size and geometry of graphene layer at the bottom. Therefore, small cracks will not affect the response drastically. Among all the proposed tunable PIT designs hybrid metal-graphene design was reasonable to experimentally realize. Therefore, in this thesis, I present the experimental demonstration of the tunable PIT-effect by hybrid metal-graphene structures.

Chapter 3

Electrically tunable Plasmon Induced Transparency

3.1 Introduction

Motivated with the previous studies of hybrid metal-graphene structures, I have numerically investigated and experimentally realized tunable PIT-effect for two different devices using hybrid metal-graphene structures. In this design, PIT-effect is demonstrated with Au strips on top of the graphene layer. The response is tuned by gating the graphene layer using ionic gating.

Both strips have their own plasmonic resonances that are controlled/adjusted by the lengths of the strips. The resonance of each strip serves as a bright mode. The detuning of these bright modes creates PIT-effect. Graphene has tight field confinement and tunable E_f in MIR region. Therefore, I have adjusted the geometrical patterns of our design to produce PIT-effect at $8.2 \mu\text{m}$, and tuned electrically using graphene layer.

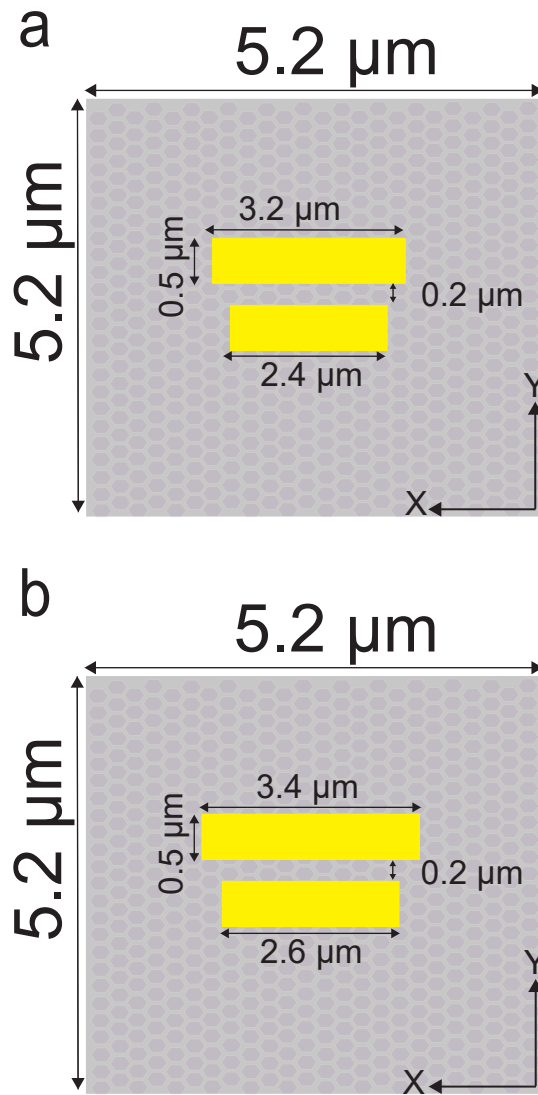


Figure 3.1: Unit cell of PIT structures, two Au strips (golden) with different lengths on graphene (grey). Both the devices have the same periodicity of $5.2 \mu\text{m}$ in x -axis and y -axis. (a) The lengths of strips are $3.2 \mu\text{m}$ and $2.4 \mu\text{m}$ for the first device. (b) The lengths of strips are $3.4 \mu\text{m}$ and $2.6 \mu\text{m}$ for the second device.

Schematics of the proposed design for first device consists of two Au strips with different lengths ($3.2 \mu\text{m}$ and $2.4 \mu\text{m}$) on top of graphene layer. Similarly, schematic of second device has Au strips but with longer dimensions ($3.4 \mu\text{m}$ and $2.6 \mu\text{m}$).

3.2 Design and Simulations

Tunable PIT devices are numerically investigated by Finite Difference Time-Domain (FDTD) method. FDTD is a numerical analysis technique that works in the time domain and can cover a long range wavelength in a single simulation. Commercially available software *Lumerical FDTD Solutions* is used to perform simulation in both transmission and reflection modes.

In my simulations, I have used periodic boundary conditions in x and y axes, while Perfect Matched Layer (PML) boundary conditions in the normal direction (z axis). Both strips have the thickness ($T=70$ nm), width ($W=0.5$ μm), and distance ($D=0.2$ μm). For the first device, I have investigated 3.2 μm and 2.4 μm long Au strips, shown in Figure 3.1 (a). For the second device, I have investigated 3.4 μm and 2.6 μm long Au strips, shown in Figure 3.1 (b).

BaF₂ is used as infinite transparent substrate and graphene is introduced as 2D dispersive material between the substrate and Au strips. In our simulations, the optical constant of the gold is considered based on Palik model and the applied optical parameters of the BaF₂ is extracted from Reference [61]. The unit cell is illuminated by a plane wave source along the z direction having electric component (E) parallel to x -axis. 3D view of our device is present in Figure 3.2 (a). Complete simulation setup is shown in Figure 3.2 (b).

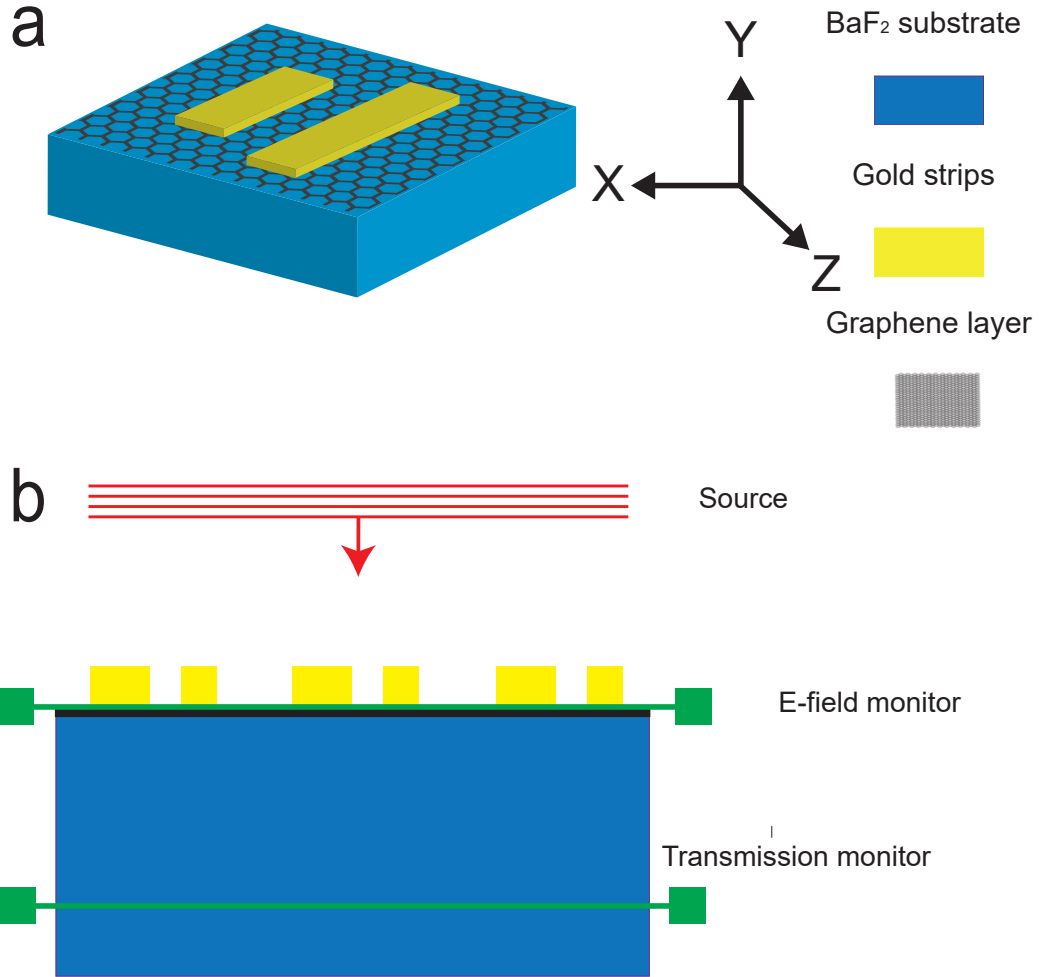


Figure 3.2: Schematic of simulation setup. (a) 3D view of PIT device, BaF_2 is used as transparent substrate with a graphene layer and Au strips on top of graphene. (b) Complete simulation setup of PIT device, plane wave source for exciting the structure, two monitors for E-field and transmission measurements.

For tuning the PIT response, E_f of graphene was changed from 0.5 eV to 0.8 eV with a step of 0.15 eV for three different simulations. Γ of graphene was set as 0.01 eV ($2.4 \times 10^{12} \text{ sec}^{-1}$), T was set as 300 K. Γ is limited by the quality of graphene, I have taken a high value for Γ to achieve comparable results with the experiments.

3.3 Fabrication Process

Both devices are fabricated using commercially available chemical vapor deposition (CVD) grown graphene on Cu. I have transferred graphene onto BaF₂ using wet transfer method, electron beam (E-beam) lithography was used to pattern the structures and E-beam evaporation was used for the deposition of metals. Details of each fabrication process are explained in the following sections.

3.3.1 Graphene transfer

A monolayer 10×10 mm² size graphene grown on Cu films from <https://graphene-supermarket.com/> was used for this work. Graphene transfer process starts with spin coating Poly (methyl methacrylate) (PMMA) A4 resist on the sample at 6000 RPM for 40 seconds with a ramp of 4. I have cut the sample into 5×5 mm². I leave the spin coated graphene for 12 hours. On the next day, I remove graphene from the bottom by leaving the sample in the solution of HNO₃: H₂O (1:3) for 3 min. Once graphene from the bottom is removed, Cu, is etched by leaving the sample in Ammonium per Sulfate (0.1 Mol) for 2 hours. For removing the residue of Cu, I leave the sample in HCL:H₂O₂:H₂O (1:1:20) solution for 15 minutes. Graphene is then transferred to de-ionized water to dilute the acids. Once the substrate is clean, I then take graphene on top of the substrate and leave it to dry for 5 minutes. Later the sample is baked at 150 degrees centigrade for 5 minutes. PMMA is removed from the top using acetone and isopropyl alcohol (IPA), Figure 3.3 shows the graphene transfer results on Si substrate.

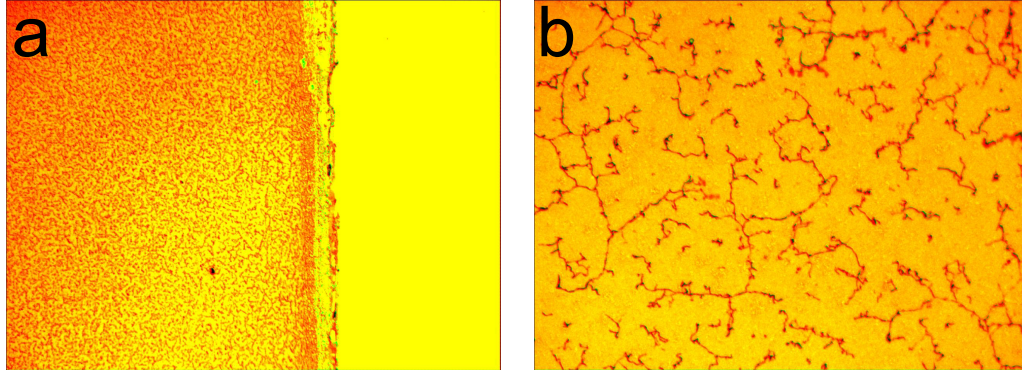


Figure 3.3: Microscope image of graphene transfer (a) Image from 5X eyepiece showing the corner of graphene layer on top of Si substrate. (b) Image from 50X eyepiece showing surface of graphene.

During the transfer process, graphene will be chemical doped, and E_f of graphene will be shifted. For finding the new value charge neutrality point (CNP) is measured. It is the point where resistance has maximum value and capacitance has minimum value for the applied voltage. It is reported to be -0.6 V and 0.5 eV in simulations previously in our lab [45]. I have used these values as reference in my simulations and experiments.

3.4 E-beam lithography

E-beam lithography is a nano fabrication technique used to pattern structures. It works on the principal of scanning the resist surface (which is used for E-beam), and pattern at nm scale. E-beam is capable of patterning the structures at smaller scale because of its short wavelengths of almost 5 nm. However, it requires experience for optimizing the resist thickness, exposure dose, developing time, and electron beam spot size for every new structure. Smallest spot size can be achieved by accurately adjusting focus and stigmation settings.

For our work, I spin coat PMMA A4 resist at 3000 RPM for 40 seconds with a ramp of 4 . The thickness of resist becomes 250 nm. After spin coating and baking the resist, I coat the sample with a conductive polymer like aquaSAVE

at the same rate. The sample is exposed to an area dose of $150 \mu\text{C}/\text{cm}^2$, and single pixel line dose of $2000 \text{ pC}/\text{cm}^2$. The working distance was 6 mm and width of the aperture was $30 \mu\text{m}$. I exposed the area of $200 \times 200 \mu\text{m}^2$ suitable for transmission measurements. Acceleration voltage of the device used is 30 KV and current was kept 350 pA. In our laboratories we are using the eLine system by Raith GmbH. After the exposure aquaSAVE is removed by rinsing under the water, resist is developed by solution of MIBK: IPA (1:1) for 1 minute and in IPA for 30 seconds. As PMMA A4 is positive resist the part which are exposed to E-beam will be removed during development process.

3.4.1 E-beam evaporation

Once the sample is patterned, I use E-beam evaporator to deposit metals. E-beam evaporation is a type of physical vapor deposition. In this process, source material (metals in our case) are evaporated using electrons accelerated from the gun towards the crucible. The process takes place in a vacuum environment. A sample holder is placed exactly above the crucible. The rate of deposition is monitor by a crystal and can be controlled by adjusting acceleration current and voltage. Schematic of E-beam evaporator is shown in Figure 3.5 [62].

5/65 nm of Ti/Au were coated on patterned samples. Both the metals were deposited at a constant rate of $1 \text{ \AA}/\text{sec}$. The pressure of the chamber was 9×10^{-6} mBa. The acceleration voltage was set at 7.28 KV. Structures appeared after the lift-off process of 24 hours in acetone. In our laboratories, we are using UNIX 350 system.

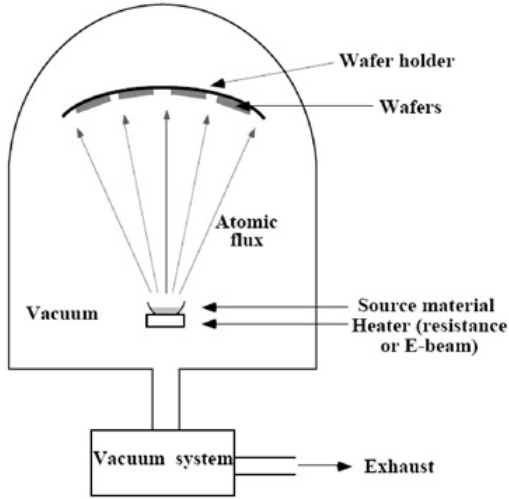


Figure 3.4: Schematic of E-beam evaporation setup. Electrons generated from ion source are accelerated towards source crucible. The materials are evaporated and deposit onto patterned sample, attached to sample holder [62].

3.4.2 Top gating

In order to apply the gate voltage to graphene, second BaF_2 substrates with the metal contacts at the corners were placed on top of PIT device and separated by an insulating tape. An ionic liquid (Diethylmethyl(2-methoxyethyl) ammonium bis(trifluoromethylsulfonyl) imide, $[\text{deme}][\text{Tf}_2\text{N}]$) is inserted between the two substrates, a source was connected to graphene layer and metal contacts using a conductive tape. By applying the gate voltage capacitance is produced between graphene layer and the gold contact due to the presence of ionic liquid [46, 45]. A schematic of top gating method is shown in Figure 3.5.

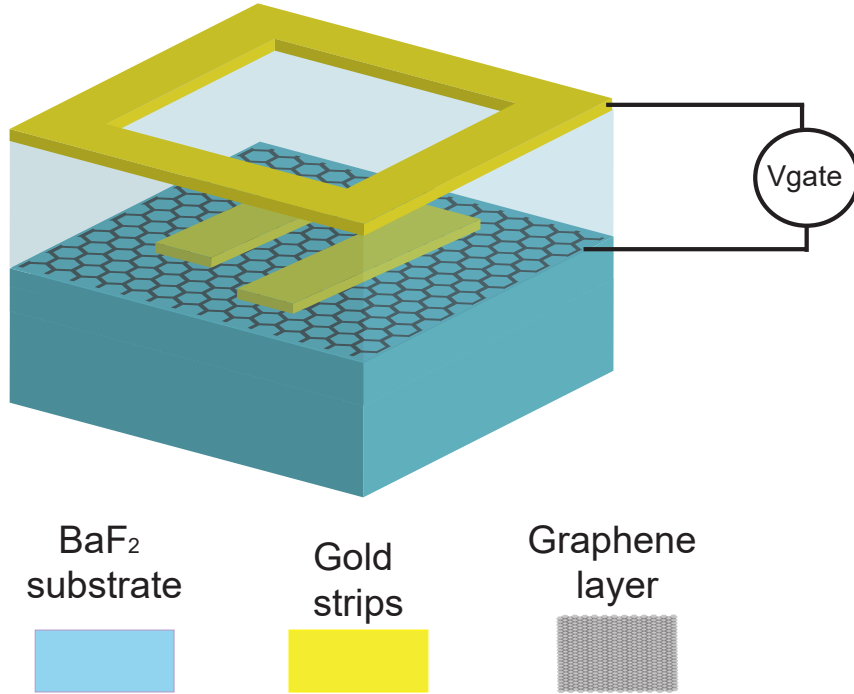


Figure 3.5: Schematic of top gating of PIT device. Two BaF₂ substrates are used. The first one with Au strips on graphene, which is connected to the source by conductive tape. The second one with a window for FTIR measurements and coated with Ti/Au, which is connected to the second terminal of the source. Ionic liquid (transparent area) is injected between these two substrates.

By controlling this induced field due to capacitance, I have controlled the carrier concentration accumulation near the surface of graphene. As discussed earlier in section 2.1.1 by E_f of graphene can be controlled by carrier concentration. The optical window for the second substrate was created using photolithography method.

3.4.3 Photolithography

Photolithography is well established micro-fabrication technique with fast and high throughput for a minimum feature size of 3 μm . The sample is coated

with a material which is sensitive to light (photoresist). When exposed to ultraviolet (UV) light will change the solubility of photoresist. A photomask is used to pattern resist and defines which part need to be exposed. Mask aligner is used to for the alignment between the sample and the mask. Feature size is dependent to the factors such as photoresist thickness, proximity/contact mode, exposure time, and development time. In this thesis, I have used image reversal photolithography because I wanted to have transparent window in the center and metals at the corners for top gating.

3.5 Characterization

3.5.1 Characterization of graphene

The quality of graphene can be characterized using well known technique of Raman spectroscopy. The most important peaks for characterization of graphene are at $\sim 1580 \text{ cm}^{-1}$ and at $\sim 2700 \text{ cm}^{-1}$, they are named as G and 2D bands, respectively. Both of these peaks are observed in graphite samples [63]. By comparing the ratio of 2D and G band number of bulk graphite or number of layers for graphene can be calculated. For monolayer graphene 2D band is 4 times intense than G band and 2 times for double layer graphene [64]. Figure 3.6 shows Raman spectroscopic results for graphene on Si substrate transferred using wet transfer method.

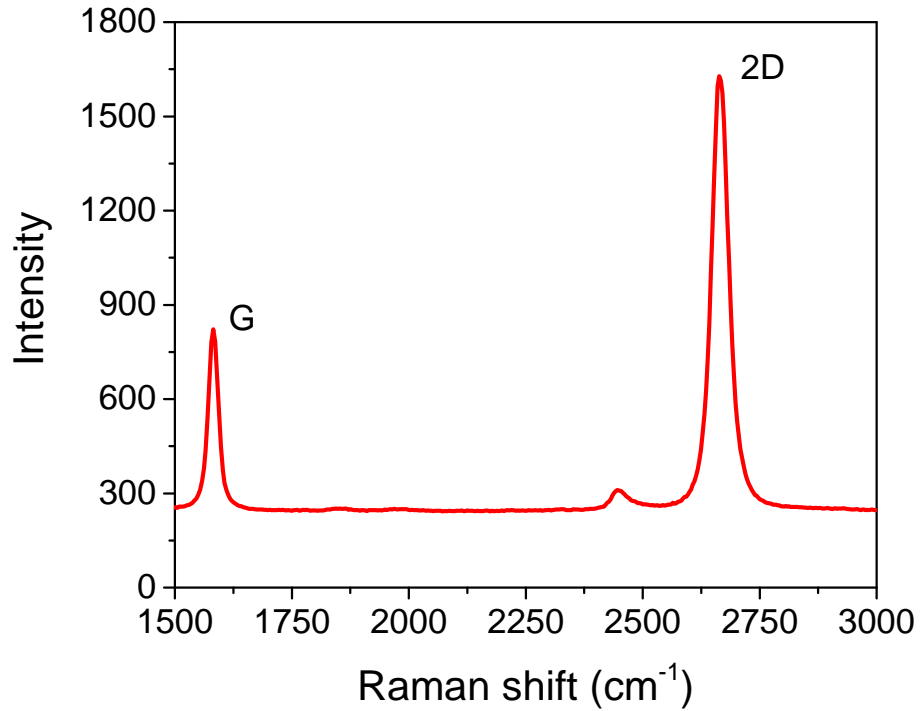


Figure 3.6: Raman signal of a graphene layer on Si sample using wet transfer method.

3.5.2 Characterization of the fabricated samples

In order to measure the surface topography and guarantee the pattern during dose the test of E-beam lithography, scanning electron microscopy (SEM) is used. SEM produces images of a sample by scanning surface and measuring secondary electron. Figure 3.7 shows the SEM images of the fabricated samples.

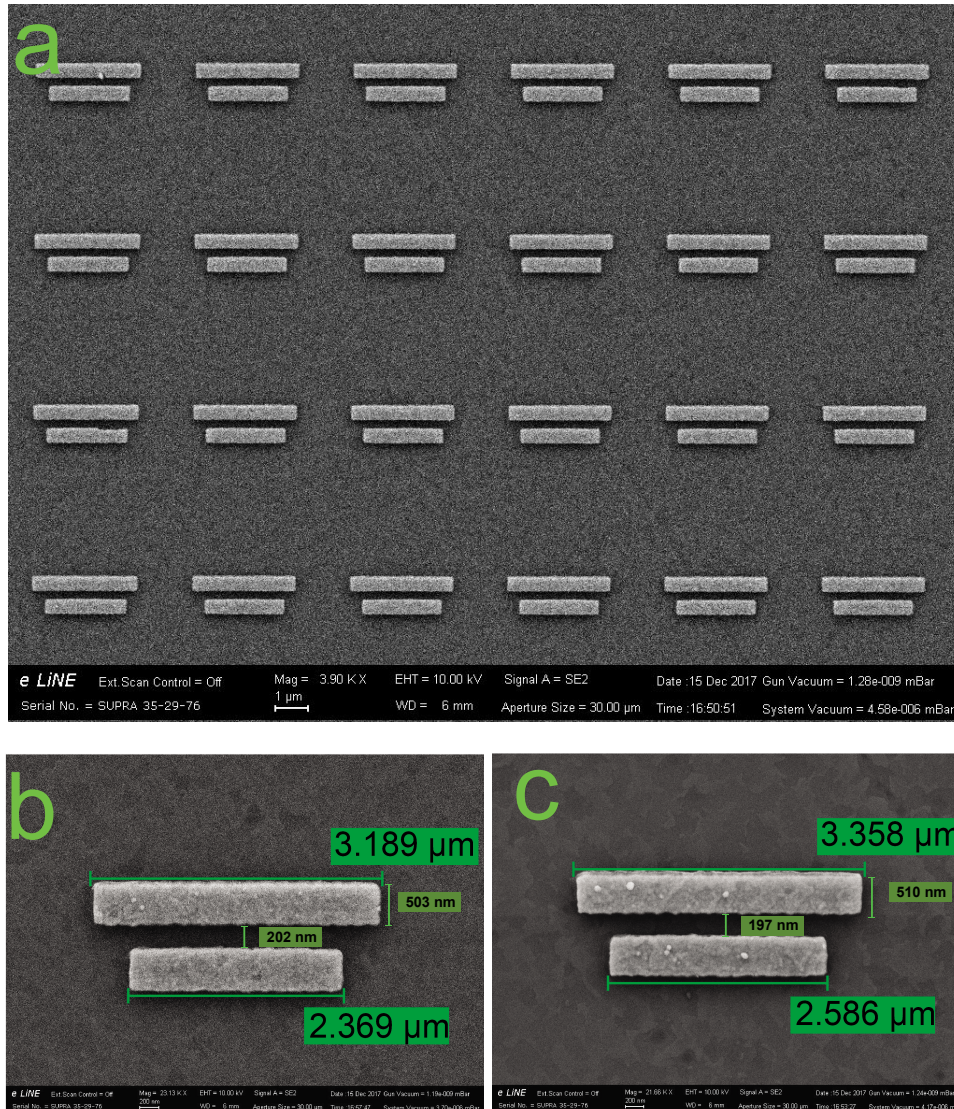


Figure 3.7: SEM images of PIT device. (a) Image for multiple unit cells. (b) SEM image of first device with shorter lengths of Au strips. (c) SEM image of second device with longer lengths of Au strips.

Three dimensional topography of sample and height is measured using atomic force microscopy. AFM technique is dependent on the forces between the tip and sample, these forces effect AFM imaging. Figure 3.8 shows the AFM results for tunable PIT device and height of the strips (70 nm).

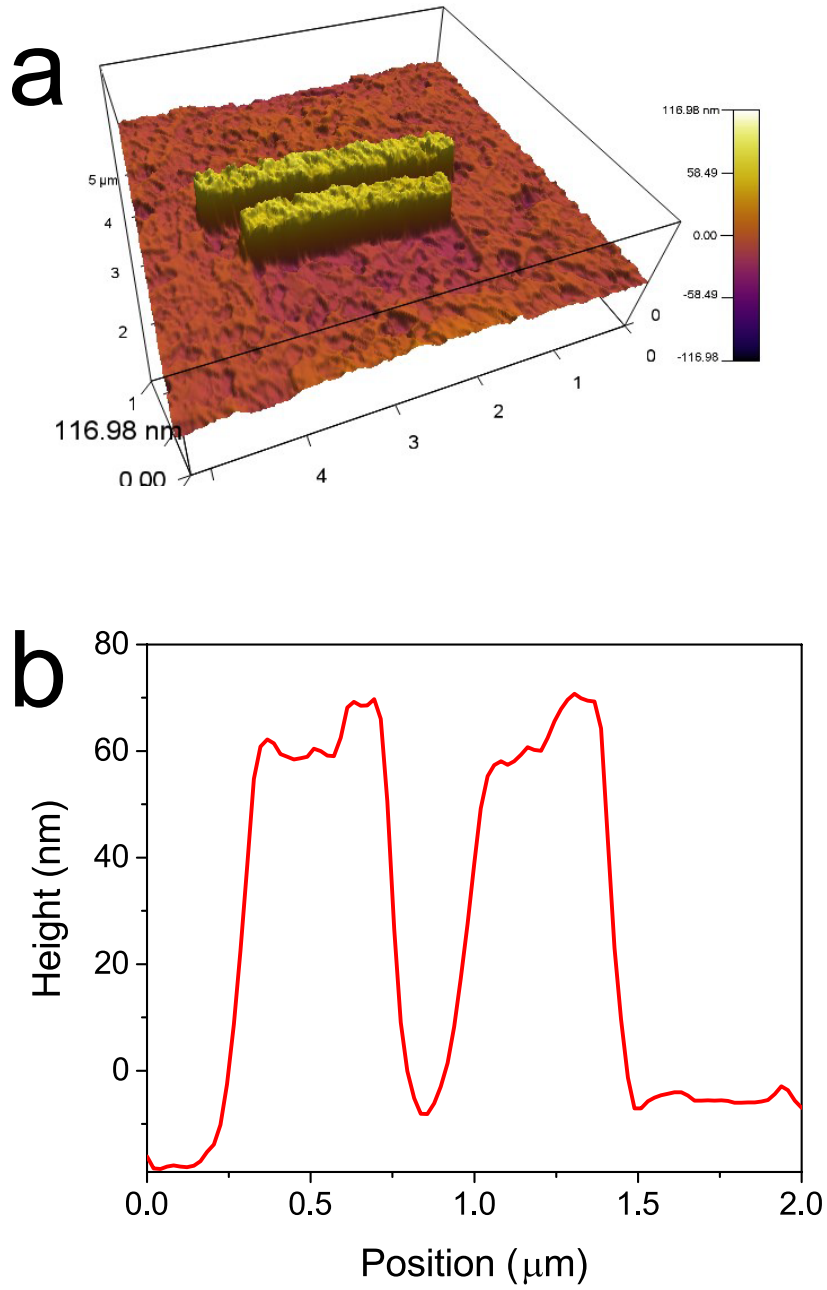


Figure 3.8: AFM measurement of PIT device. (a) 3D topography of a sample surface. (b) Height measurement of the sample, height of two strips is 70 nm.

3.6 Results

Normalized transmission measurements for two different devices were obtained by using a Fourier-transform infrared spectroscopy (FTIR) instrument integrated with a microscope. In our laboratory, we use Vertex 70V FTIR and Hyperian 2000 IT microscope. I used the microscope in order to focus individual unit of my samples $200 \times 200 \mu\text{m}^2$. For the measurement, samples were illuminated with normal incidence by MIR source and Potassium bromide (KBr) beam splitter and by x polarized field. MCT D313 detector was cooled 30 minutes by liquid nitrogen prior to the measurements. Measurements were done from 6 to 14 μm at different gate voltage using the top gating. By changing the gate voltage surface carrier concentration and E_f of graphene was changed. A shift was observed in PIT-effect. The background measurements were taken from graphene on BaF_2 substrates with no PIT structures.

The transmission simulation for each of the Au strips shows strong responses as presented in the insets of Figure 10(a) for the first device. As described above, when strips are brought close to each other, they result in a weak hybridization and give the PIT-effect presented in Figure 10(a). This response is not observed by the excitation of a single strip. Similarly, I have investigated two strips with longer dimension for the second device.

Good agreement of simulation and experimental results for changing E_f and gate voltage. The minimum gate voltage was selected based on CNP, measured previously to be -0.6 V for a similar graphene structure [45, 46]. Moreover, I have also investigated the effect of changing the dimensions. Increasing the lengths of the strips by 0.2 μm will shift the PIT-effect up to 350 nm. Comparison for the experimental results is shown in Figure 3.9.

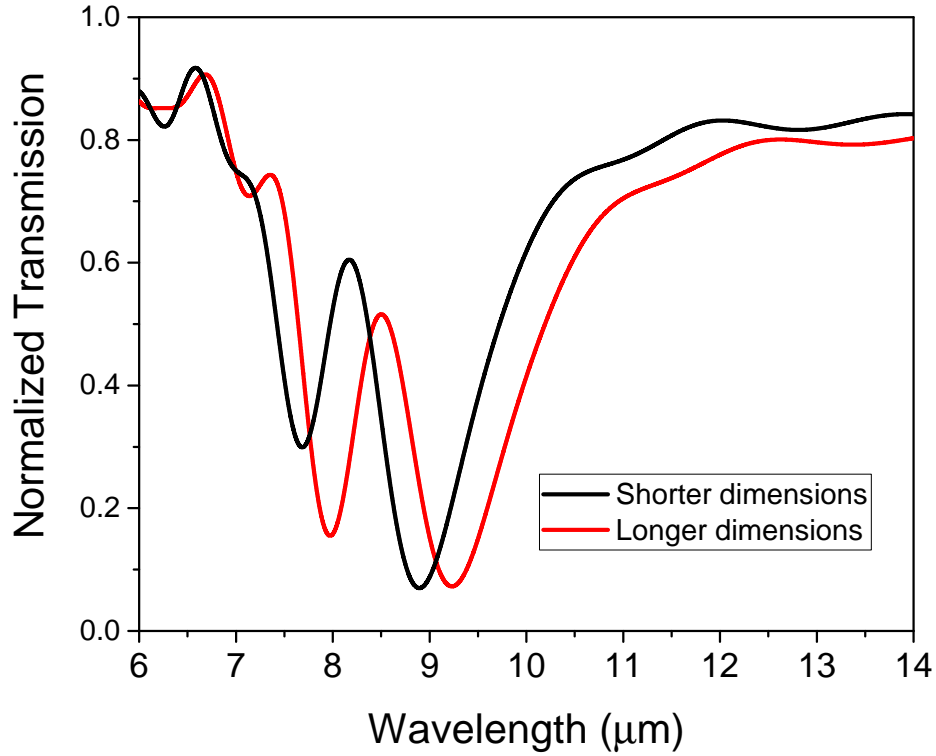


Figure 3.9: Comparison of PIT-effect for the device with shorter dimensions (black) and the device with longer dimensions (red).

By increasing the E_f of graphene from 0.5 eV to 0.8 eV the PIT response is shifted towards smaller wavelengths for both the devices. Simulation results for three different E_f of graphene for first and second device are presented in Figure 3.10 (a) and Figure 3.11 (a), respectively. Similarly, by increasing the gate voltage from CNP (-0.6 V) to 2.4 V a blue shift is observed in the PIT-effect. Normalized transmission results of FITR measurements at -0.6 V 0.9 V and 2.4 V are presented in Figure 3.10 (b) for the first device and in Figure 3.11 (b) for the second device.

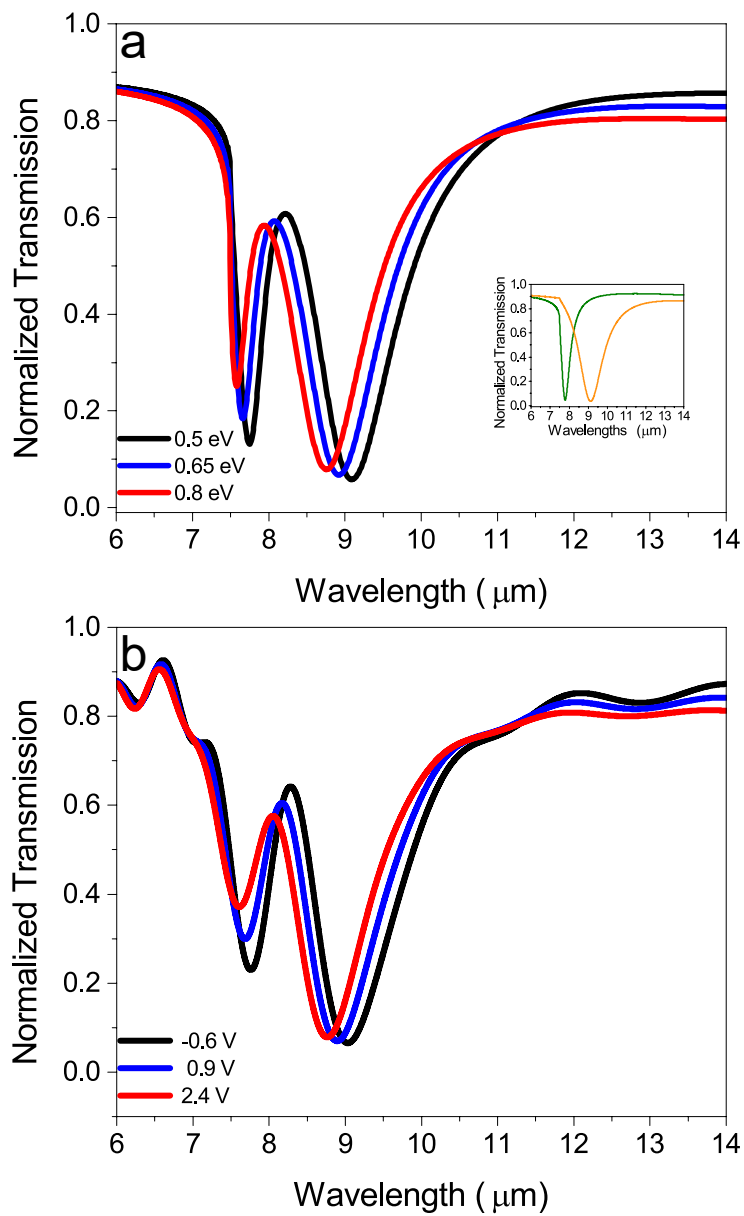


Figure 3.10: Simulated and FTIR measurement of PIT structures. (a) Simulated results of first device ($3.2 \mu\text{m}$ and $2.4 \mu\text{m}$) for different E_f . (b) Normalized transmission for first device (shorter dimensions) at -0.6 V , 0.9 V and 2.4 V .

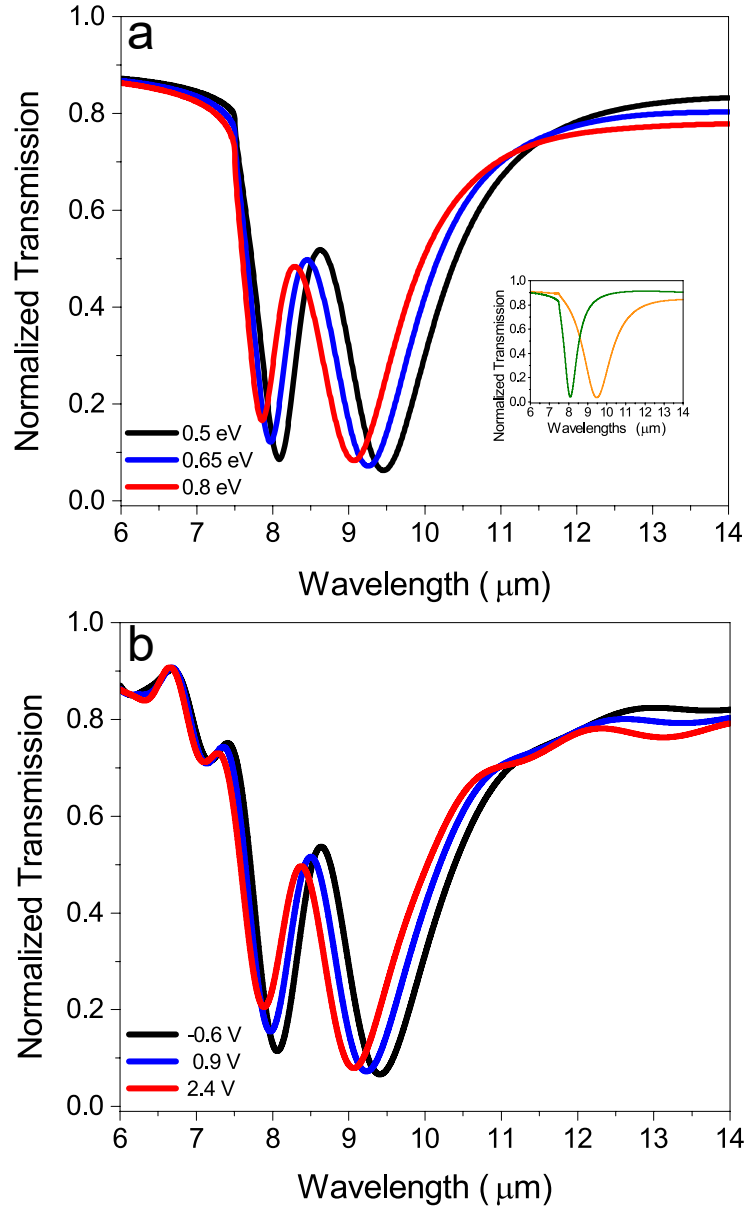


Figure 3.11: Simulated and FTIR measurement of PIT structures. (a) Simulated results of second device ($3.4 \mu\text{m}$ and $2.6 \mu\text{m}$) for different E_f . (b) Normalized transmission for second device (longer dimensions) at -0.6 V , 0.9 V and 2.4 V .

Charge density in graphene layer is increased by increasing the gate voltage from -0.6 V to 2.4 V . This will shift the resonance frequency of graphene, which is directly proportion to E_f . Therefore, blue shift is observed by increasing E_f in my design.

3.6.1 Mode profile

Investigation of Electric field for two strips with resonances at different wavelengths are investigated for the first device at 0.5 eV. Electric field magnitudes of two resonance wavelengths in the transmission spectrum ($7.75 \mu\text{m}$ and $9.06 \mu\text{m}$) are shown in Figure 3.12(a) and 3.12(c). In addition, the Electric field magnitude at a PIT wavelength is shown in Figure 3.12(b). These results show that each of the strip is excited separately at the resonance wavelengths and act as bright mode resonances. However, at $8.22 \mu\text{m}$, both strips are excited simultaneously resulting in the PIT-effect. Major localization is at the corner of the strips at their own resonance wavelengths and between two strips for transmission peak of PIT.

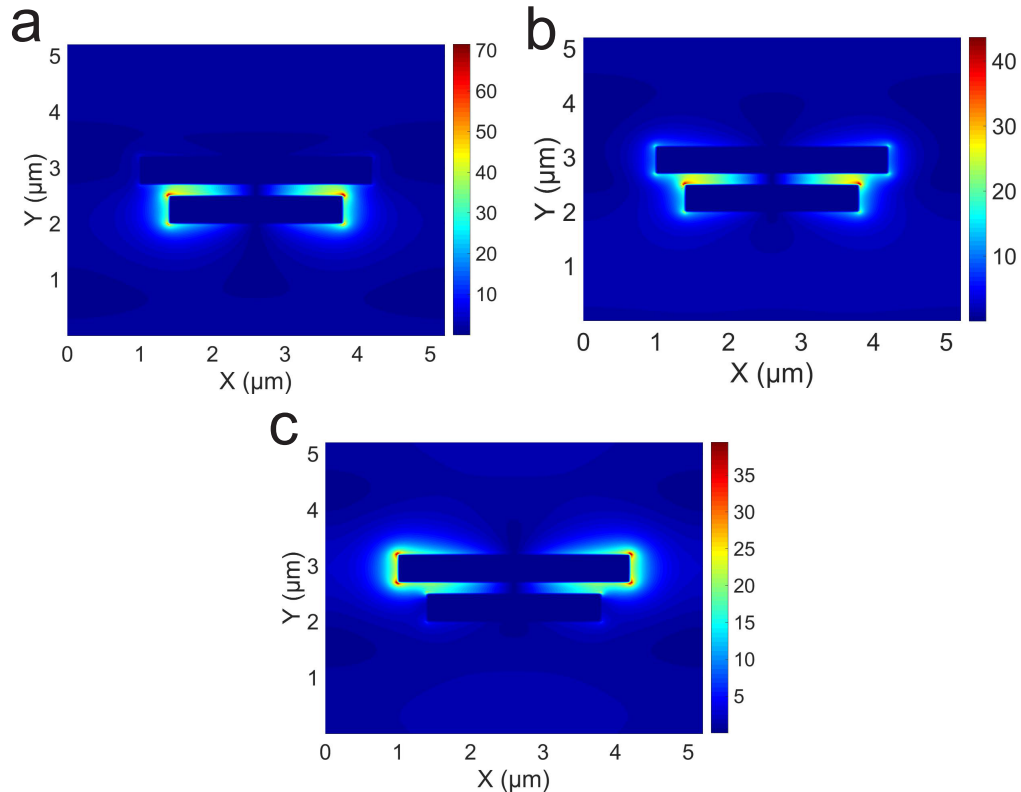


Figure 3.12: E-field magnitude for first device (shorter dimensions) at 0.5 eV (a) E-field magnitude at $7.746 \mu\text{m}$. (b) E-field magnitude at $8.217 \mu\text{m}$ (c) E-field magnitude at $9.056 \mu\text{m}$.

3.6.2 Performance

Total shift of 235 nm was observed for the first device and 263 nm for the second device by applying gate voltage of 3.0 V. Shift in PIT transmission peak at the applied gate voltage with respect to CNP is obtained for both devices and shown in Figure 3.13.

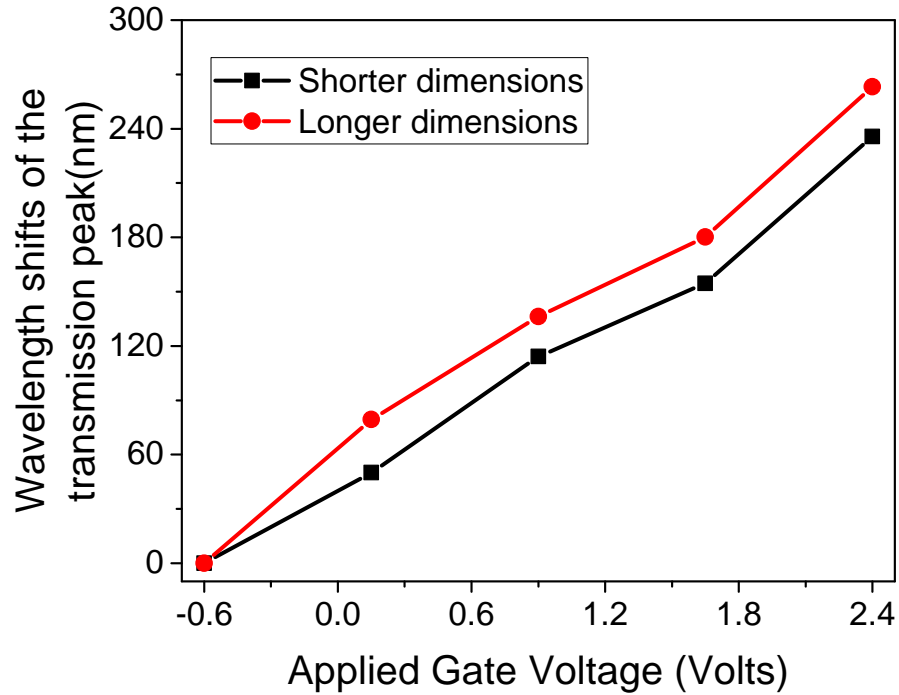


Figure 3.13: Total shift of transmission peak for device with first device (black) and second device (red).

Spectral contrast ratio (S_{con}) is used to evaluate the performance of PIT-effect [27] and described as:

$$S_{con} = \frac{(T_{peak} - T_{dip})}{(T_{peak} + T_{dip})} \times 100 \quad (3.1)$$

where T_{peak} is intensity of transmission peak and T_{dip} is intensity of resonance dip. Spectral contrast ratios of our devices are 82% and 78% for the first and second devices, respectively. Both devices with a high spectral contrast ratio and high tunability are suitable for filtering and switching applications.

3.7 Conclusion

Tunable PIT devices are numerically investigated and experimentally realized. Resonance frequencies of two strips were controlled by adjusting the length of the strips and tuned by electrically doping the graphene layer. A large tuning range was demonstrated for the FTIR measurements of PIT structures by applying gate voltage. I was able to obtain ~ 263 nm of shift in transmission window by top gating method. This concept of real time tuning PIT is exciting for novel devices in the field of optical switching, modulation, slow light applications, tunable sensors, filters, photoluminescence, and enhancing nonlinear interactions.

Chapter 4

Reflection type Tunable Plasmon Induced Transparency

4.1 Introduction

The tunable PIT design require a transparent substrate for measurements. However, for some wavelengths (MIR), limited transparent substrates are available. For measuring the PIT effect in that case, become really challenging. Therefore, reflection mode measurements are more suitable, which makes the design independent of the substrate. In this part of my thesis, I have provided an alternative method for measuring the tunable PIT effect using similar structures in reflection mode. I have proposed a reflection type PIT (RPIT) design to overcome the challenges of measurement in transmission mode.

RPIT has been realized by Ding *et al.* in 2014 [65]. In this design cut wire and split ring resonators have been used as dark and bright modes respectively. However, the design was not dynamically tunable. Therefore, I have numerically investigated and experimentally realized a hybrid metal-graphene design which generates RPIT-effect at $4.29 \mu\text{m}$, and the effect is electrically tunable.

4.2 Design and Simulations

I have numerically investigated RPIT device using FDTD method. The unit cell of the design has two parallel Au strips similar to PIT devices. Both strips are serving as two bright modes, as shown in Figure 4.1. Weak hybridization of these bright modes result in RPIT-effect. The lengths of strips are selected as $0.8 \mu\text{m}$ and $1 \mu\text{m}$, width as $W=200 \text{ nm}$ for both the strips and distance $D=200 \text{ nm}$ between the two strips. The unit cell has periodic boundary condition in x and y -axes and Perfect Matched Layers (PML) in the direction of propagation (z -axis). The design has a periodicity of $1.5 \mu\text{m}$ in x -axis and $1.0 \mu\text{m}$ in y -axis.

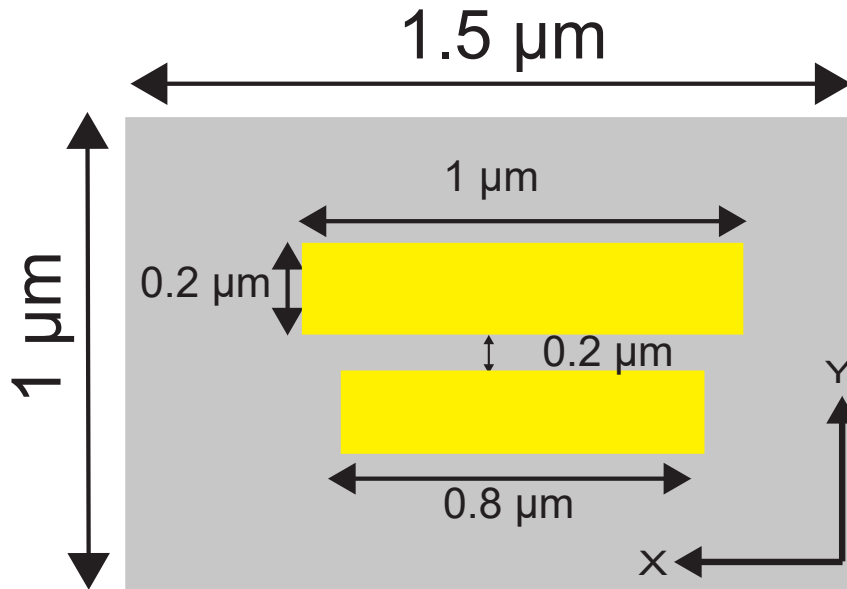


Figure 4.1: Unit cell of PIT structure. Two Au strips (golden) with lengths of $L1(0.8 \mu\text{m})$, $L2(1 \mu\text{m})$, $W(200 \text{ nm})$ is width and $D(200 \text{ nm})$ is distance between two strips. $P_x(1.5 \mu\text{m})$ and $P_y(1 \mu\text{m})$ show periodicity of unit cell.

The unit structure of device has four layers on top of Si a substrate. From top to bottom, this structure has 50 nm thick Au strips, graphene layer as 2D dispersive material, 50 nm of aluminum oxide (Al_2O_3) layer and 100 nm of reflecting aluminum (Al) layer, shown in Figure 4.2. A plane wave source along the z direction was used to illuminate the unit cell having the electric field component

(E) parallel to x -axis. For tuning the RPIT response, three different values of E_f for graphene were investigated. Also for this work, (Γ) of graphene was set as 0.01 eV ($2.4 \times 10^{12} \text{ sec}^{-1}$), temperature (T) was set as 300 K.

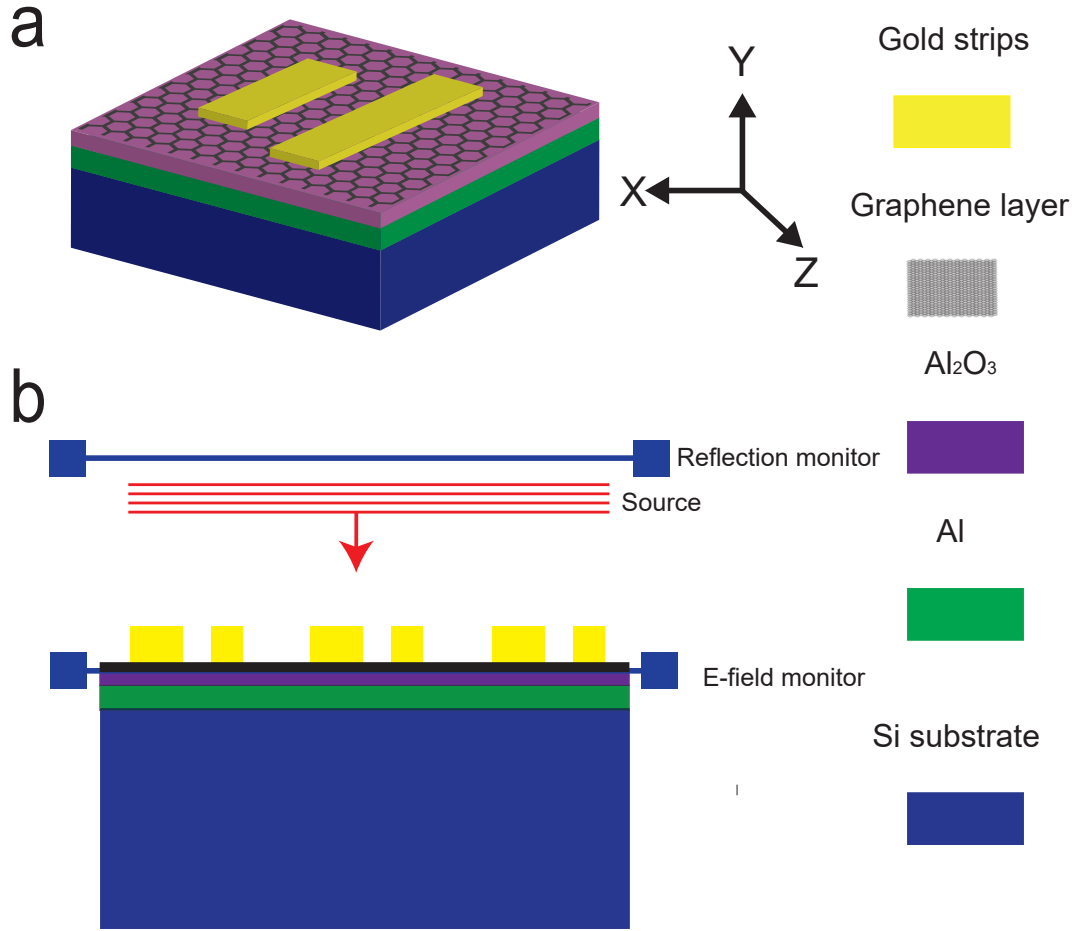


Figure 4.2: Schematic of simulation setup. (a) 3D view of RPIT device, Si is used as substrate with an Al and Al₂O₃ for reflective and dielectric layers. Au strips on top of graphene. (b) Complete simulation setup with a RPIT device, plane wave source for exciting the structure, two monitors for E-field and reflection measurements.

4.3 Fabrication

RPIT device is also fabricated using commercially available CVD grown graphene on Cu. Si substrate is cleaned using oxygen plasma at 100 W radio frequency (RF) power for 2 minutes to clean the residue of deicing resist. Al is deposited using E-beam evaporator at the rate of 1.2 Å/sec. Al₂O₃ is deposited using atomic layer deposition (ALD). ALD is a subclass of CVD, chemical reaction take place on the surface to form 1 nm thick oxide layer in each step. The process results in highly uniform thin films because of the slow rate. I have transferred graphene on top of the oxide layer with wet transfer method as discussed in section 3.3.

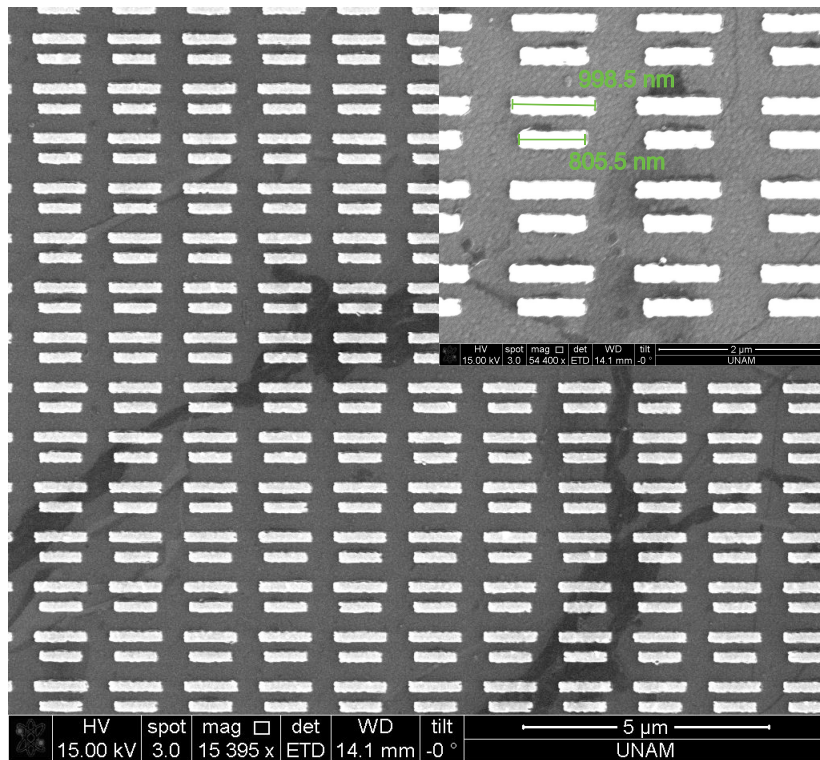


Figure 4.3: SEM images of RPIT structures.

For RPIT, I have spin coated PMMA A4 resist at 3000 RPM for 40 seconds with a ramp of 4. The thickness of resist becomes 250 nm. After spin coating and baking the resist, sample is coated with a conductive polymer like aquaSAVE with the same rate. The sample is exposed to an area dose of 150 μC/cm², and

single pixel line dose of 2000 pC/cm². The working distance was 6 mm and width of the aperture was 30 μm . I have exposed an area of 250 \times 20 μm^2 this time, suitable for reflection measurements. The acceleration voltage of device used is 30 KV and a current was kept 350 pA. After the exposure aquaSAVE is removed by rinsing under the water, resist is developed by a solution of MIBK: IPA (1:1) for 1 minute and in IPA for 30 sec.

Once the sample is patterned, 5/50 nm of Ti/Au were coated on patterned samples. Both the metals were deposited at a constant rate of 1.2 $\text{\AA}/\text{sec}$. The pressure of chamber was 9×10^{-6} mBa. Acceleration voltage was set as 7.28 V. Structures appeared after the lift-off process of 24 hours in acetone. SEM images of RPIT structures is shown in Figure 4.3. Top gating method was used to tune RPIT response of the device.

4.4 Results

Reflection measurements for RPIT device was obtained by using a FTIR instrument integrated with a microscope. For the measurement, samples were illuminated with normal incidence by MIR source by KBr beam splitter and by x polarized field. MCT D313 detector was cooled 30 minutes by liquid nitrogen prior to measurement. Measurements were done from 2.5 to 6.5 μm at different gate voltages using the top gating. The background measurements were taken from Au mirror.

The reflection simulation and experimental results are presented in Figure 4.4. This response is shifted toward shorter wavelengths as E_f of graphene is increased, shown in Figure 4.4(a). As the gate voltage is increased from -0.6 V to 2.4 V, a blue shift is observed in RPIT-effect, shown in Figure 4.4(b).

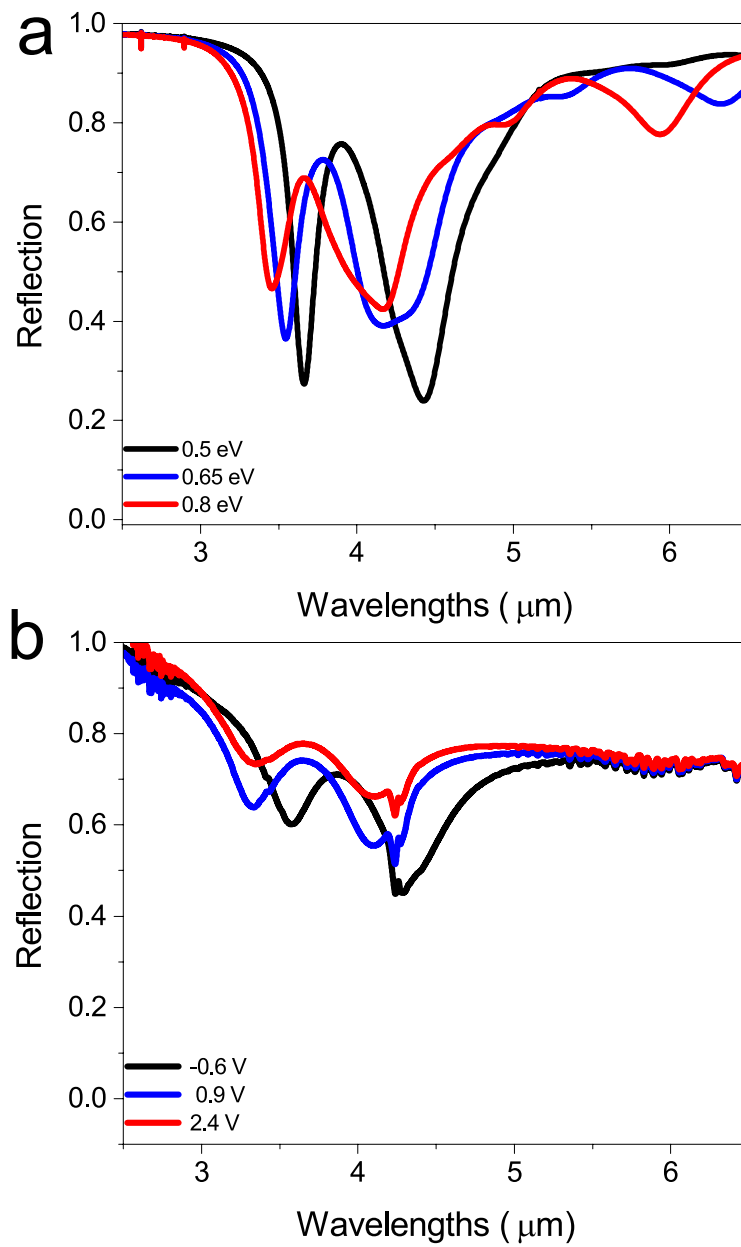


Figure 4.4: Simulated and FTIR measurement of RPIT structures. (a) Simulated results for different E_f . (b) Normalized transmission at -0.6 V, 0.9 V and 2.4 V.

4.4.1 Mode profile

E-field investigation of two strips was made for three different wavelengths, shown in Figure 4.5. Electric field magnitudes were presented at of two resonance wavelengths (3.65 μm and 4.42 μm) in Fig. 2(a) and 2(c). Moreover, the E-field magnitude is shown at RPIT wavelength (3.87 μm) in Figure 4.5(b).

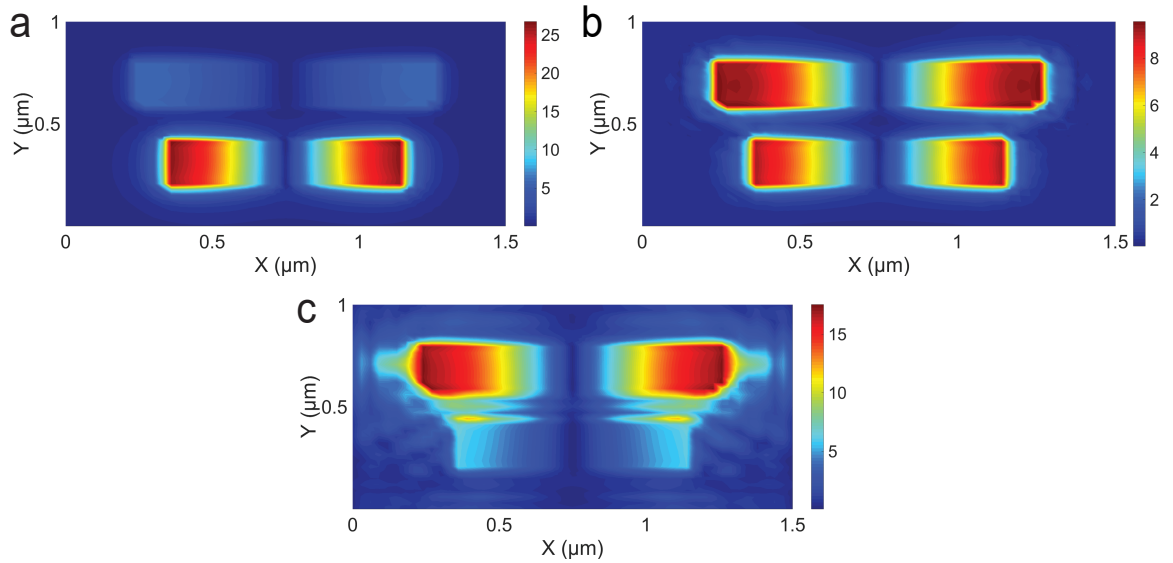


Figure 4.5: E-field magnitude at 0.5 eV (a) E-field magnitude at 3.65 μm . (b) E-field magnitude at 4.420 μm (c) E-field magnitude at 3.87 μm

4.4.2 Performance

Total shift of 220.8 nm was observed by changing gate voltage of 3.0 V. Spectral contrast ratio (S_{con}) for RPIT is described as:

$$S_{con} = \frac{(R_{peak} - R_{dip})}{(R_{peak} + R_{dip})} \times 100 \quad (4.1)$$

where R_{peak} is intensity of reflection peak and R_{dip} is intensity of resonance dip. S_{con} of our design is 22.56%. The device is suitable for filtering and switching applications.

4.5 Conclusion

RPIT has been numerically investigated and experimentally using two strips on top of graphene. By changing E_f of graphene PIT in reflection was shifted. A large tuning range was demonstrated for the FTIR measurements of RPIT structures by applying gate voltage. I was able to obtain 220.8 nm of shift in transmission window by applying gate voltage from up to 3 V. These results of RPIT can be used in many fields such as slow light applications and nonlinear optics.

Chapter 5

Conclusion and Outlook

PIT and RPIT-effect can be realized by a simple design of metamaterials on top of an active material such as graphene. The devices realized earlier were based on the metallic element which limits tunability. On the other hand, the numerical investigations of tunable designs were too complex to be realized. However, a hybrid metal-graphene structure has overcome both the problems. Moreover, ~ 250 nm (1200 THz) shift was observed by top gating method which is an efficient tuning mechanism at low operating voltages (3 V).

I have numerically investigated and experimentally realized tunable PIT-effect using two Au strips on graphene. Each strip serves as bright mode and produces a plasmonic resonance. These resonances are tunable as E_f of graphene is changed by electrostatic doping. I have numerically investigated two devices for tunable PIT-effect using FDTD method. The PIT-effect is controlled by adjusting the lengths of the strips. The PIT-effect is shifted towards the shorter wavelengths by increasing the E_f of graphene. For experiments, the devices were fabricated using wet transfer method of graphene onto a transparent BaF₂ substrate. Raman spectroscopy is used to investigate the quality of graphene. Au strips are fabricated on top of the graphene layer. Normalized transmission experiments are done using FTIR device integrated with a microscope in MIR range. E_f of graphene was changed by applying gate voltage using top gating method. Total

shift of 263 nm was observed in PIT-effect and spectral contrast ratios of our devices are 82% and 78% for shorter and longer dimensions, respectively.

In addition, I have also numerically investigated and experimentally realized tunable PIT-effect in reflection mode, the RPIT-effect was also produced by de-tuning of two bright modes. I numerically investigated four layers design with a metal layer at the bottom for reflection, a dielectric layer as spacer, graphene layer and Au strips on top to produce tunable RPIT-effect. Total shift of 220.8 nm was observed in RPIT-effect and spectral contrast ratios of our device is 22.56%.

Overall, I propose an electrically tunable PIT and RPIT devices that is based on novel metal-graphene metamaterials which can be used for tunable enhanced sensing and switchable systems. As in these investigations, two devices in the transmission modes and one in reflection mode for different dimensions, the response is controlled by geometrical patterns. The wavelength of operation can also be altered by the size and shape of the structures and tuned by active material like graphene. Moreover, other hybrid designs which are tunable by heat or light can be investigated with the same structures.

Bibliography

- [1] T. F. Krauss, “Why do we need slow light?,” *Nature Photonics*, vol. 2, no. 8, p. 448, 2008.
- [2] Y. Huang, C. Min, and G. Veronis, “Subwavelength slow-light waveguides based on a plasmonic analogue of electromagnetically induced transparency,” *Applied Physics Letters*, vol. 99, no. 14, p. 143117, 2011.
- [3] G. Wang, H. Lu, and X. Liu, “Dispersionless slow light in mim waveguide based on a plasmonic analogue of electromagnetically induced transparency,” *Optics express*, vol. 20, no. 19, pp. 20902–20907, 2012.
- [4] M. Fleischhauer, A. Imamoglu, and J. P. Marangos, “Electromagnetically induced transparency: Optics in coherent media,” *Reviews of modern physics*, vol. 77, no. 2, p. 633, 2005.
- [5] J. Chen, P. Wang, C. Chen, Y. Lu, H. Ming, and Q. Zhan, “Plasmonic eit-like switching in bright-dark-bright plasmon resonators,” *Optics express*, vol. 19, no. 7, pp. 5970–5978, 2011.
- [6] R. D. Kekatpure, E. S. Barnard, W. Cai, and M. L. Brongersma, “Phase-coupled plasmon-induced transparency,” *Physical review letters*, vol. 104, no. 24, p. 243902, 2010.
- [7] I. Novikova, R. L. Walsworth, and Y. Xiao, “Electromagnetically induced transparency-based slow and stored light in warm atoms,” *Laser & Photonics Reviews*, vol. 6, no. 3, pp. 333–353, 2012.

- [8] Z.-G. Dong, H. Liu, J.-X. Cao, T. Li, S.-M. Wang, S.-N. Zhu, and X. Zhang, “Enhanced sensing performance by the plasmonic analog of electromagnetically induced transparency in active metamaterials,” *Applied Physics Letters*, vol. 97, no. 11, p. 114101, 2010.
- [9] Z. Vafapour, Y. Hajati, M. Hajati, and H. Ghahraloud, “Graphene-based mid-infrared biosensor,” *JOSA B*, vol. 34, no. 12, pp. 2586–2592, 2017.
- [10] Z. Vafapour, “Near infrared biosensor based on classical electromagnetically induced reflectance (cl-eir) in a planar complementary metamaterial,” *Optics Communications*, vol. 387, pp. 1–11, 2017.
- [11] Y. Wu, J. Saldana, and Y. Zhu, “Large enhancement of four-wave mixing by suppression of photon absorption from electromagnetically induced transparency,” *Physical Review A*, vol. 67, no. 1, p. 013811, 2003.
- [12] K.-J. Boller, A. Imamoglu, and S. E. Harris, “Observation of electromagnetically induced transparency,” *Physical Review Letters*, vol. 66, no. 20, p. 2593, 1991.
- [13] S. Harris, J. Field, and A. Kasapi, “Dispersive properties of electromagnetically induced transparency,” *Physical Review A*, vol. 46, no. 1, p. R29, 1992.
- [14] A. Kasapi, M. Jain, G. Yin, and S. E. Harris, “Electromagnetically induced transparency: propagation dynamics,” *Physical review letters*, vol. 74, no. 13, p. 2447, 1995.
- [15] J. P. Marangos, “Electromagnetically induced transparency,” *J. Mod. Opt.*, vol. 45, no. 3, pp. 471–503, 1998.
- [16] C. Rohde, K. Hasegawa, and M. Deutsch, “Plasmon-assisted transparency in metal-dielectric microspheres,” *Optics letters*, vol. 32, no. 4, pp. 415–417, 2007.
- [17] V. Yannopapas, E. Paspalakis, and N. V. Vitanov, “Electromagnetically induced transparency and slow light in an array of metallic nanoparticles,” *Physical Review B*, vol. 80, no. 3, p. 035104, 2009.

- [18] N. Papasimakis, V. A. Fedotov, N. Zheludev, and S. Prosvirnin, “Metamaterial analog of electromagnetically induced transparency,” *Physical Review Letters*, vol. 101, no. 25, p. 253903, 2008.
- [19] P. Tassin, L. Zhang, T. Koschny, E. Economou, and C. M. Soukoulis, “Low-loss metamaterials based on classical electromagnetically induced transparency,” *Physical review letters*, vol. 102, no. 5, p. 053901, 2009.
- [20] N. Liu, L. Langguth, T. Weiss, J. Kästel, M. Fleischhauer, T. Pfau, and H. Giessen, “Plasmonic analogue of electromagnetically induced transparency at the drude damping limit,” *Nature materials*, vol. 8, no. 9, p. 758, 2009.
- [21] Y. Zhu, X. Hu, Y. Fu, H. Yang, and Q. Gong, “Ultralow-power and ultrafast all-optical tunable plasmon-induced transparency in metamaterials at optical communication range,” *Scientific reports*, vol. 3, p. 2338, 2013.
- [22] M. P. Hokmabadi, E. Philip, E. Rivera, P. Kung, and S. M. Kim, “Plasmon-induced transparency by hybridizing concentric-twisted double split ring resonators,” *Scientific reports*, vol. 5, p. 15735, 2015.
- [23] T. Liu, “Active manipulation of electromagnetically induced transparency in a terahertz hybrid metamaterial,” *arXiv preprint arXiv:1803.06611*, 2018.
- [24] Y. Zhu, X. Hu, H. Yang, and Q. Gong, “On-chip plasmon-induced transparency based on plasmonic coupled nanocavities,” *Scientific reports*, vol. 4, p. 3752, 2014.
- [25] J. Zhang, W. Bai, L. Cai, Y. Xu, G. Song, and Q. Gan, “Observation of ultra-narrow band plasmon induced transparency based on large-area hybrid plasmon-waveguide systems,” *Applied Physics Letters*, vol. 99, no. 18, p. 181120, 2011.
- [26] Y. A. Vlasov, M. O’boyle, H. F. Hamann, and S. J. McNab, “Active control of slow light on a chip with photonic crystal waveguides,” *Nature*, vol. 438, no. 7064, p. 65, 2005.

- [27] X. Yan, T. Wang, S. Xiao, T. Liu, H. Hou, L. Cheng, and X. Jiang, “Dynamically controllable plasmon induced transparency based on hybrid metal-graphene metamaterials,” *Scientific reports*, vol. 7, no. 1, p. 13917, 2017.
- [28] M. Habib, A. R. Rashed, E. Ozbay, and H. Caglayan, “Graphene-based tunable plasmon induced transparency in gold strips,” *Optical Materials Express*, vol. 8, no. 4, pp. 1069–1074, 2018.
- [29] K. S. Novoselov, A. K. Geim, S. Morozov, D. Jiang, M. Katsnelson, I. Grigorieva, S. Dubonos, and A. Firsov, “Two-dimensional gas of massless dirac fermions in graphene,” *nature*, vol. 438, no. 7065, p. 197, 2005.
- [30] K. S. Novoselov, A. K. Geim, S. V. Morozov, D. Jiang, Y. Zhang, S. V. Dubonos, I. V. Grigorieva, and A. A. Firsov, “Electric field effect in atomically thin carbon films,” *science*, vol. 306, no. 5696, pp. 666–669, 2004.
- [31] K. Novoselov, D. Jiang, F. Schedin, T. Booth, V. Khotkevich, S. Morozov, and A. Geim, “Two-dimensional atomic crystals,” *Proceedings of the National Academy of Sciences of the United States of America*, vol. 102, no. 30, pp. 10451–10453, 2005.
- [32] X. Du, I. Skachko, A. Barker, and E. Y. Andrei, “Approaching ballistic transport in suspended graphene,” *Nature nanotechnology*, vol. 3, no. 8, p. 491, 2008.
- [33] F. Wang, Y. Zhang, C. Tian, C. Girit, A. Zettl, M. Crommie, and Y. R. Shen, “Gate-variable optical transitions in graphene,” *science*, vol. 320, no. 5873, pp. 206–209, 2008.
- [34] Z. Li, E. A. Henriksen, Z. Jiang, Z. Hao, M. C. Martin, P. Kim, H. Stormer, and D. N. Basov, “Dirac charge dynamics in graphene by infrared spectroscopy,” *Nature Physics*, vol. 4, no. 7, p. 532, 2008.
- [35] Y. Zhang, Y.-W. Tan, H. L. Stormer, and P. Kim, “Experimental observation of the quantum hall effect and berry’s phase in graphene,” *nature*, vol. 438, no. 7065, p. 201, 2005.

- [36] C. Lee, X. Wei, J. W. Kysar, and J. Hone, “Measurement of the elastic properties and intrinsic strength of monolayer graphene,” *science*, vol. 321, no. 5887, pp. 385–388, 2008.
- [37] K. Novoselov, S. Morozov, T. Mohinddin, L. Ponomarenko, D. Elias, R. Yang, I. Barbolina, P. Blake, T. Booth, and D. Jiang, “Electronic properties of graphene,” *physica status solidi (b)*, vol. 244, no. 11, pp. 4106–4111, 2007.
- [38] V. E. Dorgan, M.-H. Bae, and E. Pop, “Mobility and saturation velocity in graphene on SiO_2 ,” *Applied Physics Letters*, vol. 97, no. 8, p. 082112, 2010.
- [39] K. F. Mak, L. Ju, F. Wang, and T. F. Heinz, “Optical spectroscopy of graphene: from the far infrared to the ultraviolet,” *Solid State Communications*, vol. 152, no. 15, pp. 1341–1349, 2012.
- [40] V. Gusynin, S. Sharapov, and J. Carbotte, “Unusual microwave response of dirac quasiparticles in graphene,” *Physical review letters*, vol. 96, no. 25, p. 256802, 2006.
- [41] O. Balci, E. O. Polat, N. Kakenov, and C. Kocabas, “Graphene-enabled electrically switchable radar-absorbing surfaces,” *Nature communications*, vol. 6, p. 6628, 2015.
- [42] G. W. Hanson, “Dyadic green’s functions and guided surface waves for a surface conductivity model of graphene,” *Journal of Applied Physics*, vol. 103, no. 6, p. 064302, 2008.
- [43] Y. Yao, R. Shankar, M. A. Kats, Y. Song, J. Kong, M. Loncar, and F. Capasso, “Electrically tunable metasurface perfect absorbers for ultrathin mid-infrared optical modulators,” *Nano letters*, vol. 14, no. 11, pp. 6526–6532, 2014.
- [44] B. Guo, L. Fang, B. Zhang, and J. R. Gong, “Graphene doping: a review,” *Insciences J.*, vol. 1, no. 2, pp. 80–89, 2011.

- [45] O. Ozdemir, A. M. Aygar, O. Balci, C. Kocabas, H. Caglayan, and E. Ozbay, “Enhanced tunability of v-shaped plasmonic structures using ionic liquid gating and graphene,” *Carbon*, vol. 108, pp. 515–520, 2016.
- [46] A. M. Aygar, O. Balci, S. Cakmakyapan, C. Kocabas, H. Caglayan, and E. Ozbay, “Comparison of back and top gating schemes with tunable graphene fractal metasurfaces,” *ACS Photonics*, vol. 3, no. 12, pp. 2303–2307, 2016.
- [47] Q. Bao and K. P. Loh, “Graphene photonics, plasmonics, and broadband optoelectronic devices,” *ACS nano*, vol. 6, no. 5, pp. 3677–3694, 2012.
- [48] K. L. Kelly, E. Coronado, L. L. Zhao, and G. C. Schatz, “The optical properties of metal nanoparticles: the influence of size, shape, and dielectric environment,” 2003.
- [49] E. Prodan, C. Radloff, N. J. Halas, and P. Nordlander, “A hybridization model for the plasmon response of complex nanostructures,” *science*, vol. 302, no. 5644, pp. 419–422, 2003.
- [50] M. I. Stockman, S. V. Faleev, and D. J. Bergman, “Localization versus delocalization of surface plasmons in nanosystems: can one state have both characteristics?,” *Physical review letters*, vol. 87, no. 16, p. 167401, 2001.
- [51] A. E. Miroshnichenko, S. Flach, and Y. S. Kivshar, “Fano resonances in nanoscale structures,” *Reviews of Modern Physics*, vol. 82, no. 3, p. 2257, 2010.
- [52] S. Zhang, D. A. Genov, Y. Wang, M. Liu, and X. Zhang, “Plasmon-induced transparency in metamaterials,” *Physical Review Letters*, vol. 101, no. 4, p. 047401, 2008.
- [53] J. Xie, X. Zhu, X. Zang, Q. Cheng, Y. Ye, and Y. Zhu, “High extinction ratio electromagnetically induced transparency analogue based on the radiation suppression of dark modes,” *Scientific Reports*, vol. 7, no. 1, p. 11291, 2017.

- [54] H. Zhang, Y. Cao, Y. Liu, Y. Li, and Y. Zhang, “A novel graphene metamaterial design for tunable terahertz plasmon induced transparency by two bright mode coupling,” *Optics Communications*, vol. 391, pp. 9–15, 2017.
- [55] H. Zhang, Y. Cao, Y. Liu, Y. Li, and Y. Zhang, “Electromagnetically induced transparency based on cascaded π -shaped graphene nanostructure,” *Plasmonics*, vol. 12, no. 6, pp. 1833–1839, 2017.
- [56] G.-L. Fu, X. Zhai, H.-J. Li, S.-X. Xia, and L.-L. Wang, “Tunable plasmon-induced transparency based on bright-bright mode coupling between two parallel graphene nanostrips,” *Plasmonics*, vol. 11, no. 6, pp. 1597–1602, 2016.
- [57] H. Chen, H. Zhang, M. Liu, Y. Zhao, X. Guo, and Y. Zhang, “Realization of tunable plasmon-induced transparency by bright-bright mode coupling in dirac semimetals,” *Optical Materials Express*, vol. 7, no. 9, pp. 3397–3407, 2017.
- [58] H. Zhang, X. Zhang, Y. Cao, B. Zeng, M. Zhou, and Y. Zhang, “Tunable terahertz electromagnetically induced transparency based on a complementary graphene metamaterial,” *Materials Research Express*, vol. 4, no. 1, p. 015002, 2017.
- [59] H. Zhuang, F. Kong, K. Li, and S. Sheng, “Graphene-based electromagnetically induced transparency with coupling fabry–perot resonators,” *Applied optics*, vol. 54, no. 24, pp. 7455–7461, 2015.
- [60] B. Wei, H. Liu, G. Ren, Y. Yang, S. Ye, L. Pei, and S. Jian, “Graphene based silicon–air grating structure to realize electromagnetically-induced-transparency and slow light effect,” *Physics Letters A*, vol. 381, no. 3, pp. 160–165, 2017.
- [61] H. Li, “Refractive index of alkaline earth halides and its wavelength and temperature derivatives,” *Journal of Physical and Chemical Reference Data*, vol. 9, no. 1, pp. 161–290, 1980.
- [62] P. B. Griffin, J. D. Plummer, and M. D. Deal, “Silicon vlsi technology: fundamentals, practice, and modeling,” *1a edição*, Prentice Hall Inc, 2000.

- [63] R. Vidano, D. Fischbach, L. Willis, and T. Loehr, “Observation of raman band shifting with excitation wavelength for carbons and graphites,” *Solid State Communications*, vol. 39, no. 2, pp. 341–344, 1981.
- [64] A. C. Ferrari, J. Meyer, V. Scardaci, C. Casiraghi, M. Lazzeri, F. Mauri, S. Piscanec, D. Jiang, K. Novoselov, S. Roth, *et al.*, “Raman spectrum of graphene and graphene layers,” *Physical review letters*, vol. 97, no. 18, p. 187401, 2006.
- [65] D. Chun-Feng, Z. Ya-Ting, Y. Jian-Quan, S. Chong-Ling, X. De-Gang, and Z. Gui-Zhong, “Reflection-type electromagnetically induced transparency analogue in terahertz metamaterials,” *Chinese Physics B*, vol. 23, no. 12, p. 124203, 2014.

Appendix A

Publications

1. Habib, M., Rashed, R.A., Ozbay, E., and Caglayan, H. (2018). Graphene-based tunable plasmon induced transparency in gold strips. *Opt. Mater. Express* 8(4), 1069-1074.
2. Rashed, R.A., Gudulluoglu, B., Yun, H. W., Habib, M., Boyaci, I. H., Hong, S. H., Ozbay, E., and Caglayan, H. Highly-Sensitivity Refractive Index Sensing by Near-infrared Metatronic Nanocircuits. (Submitted)
3. Habib, M., Ozbay, E., and Caglayan, H. Tunable Reflection Type Plasmon Induced Transparency with Graphene. (Submitted to Metamaterials 2018 Conference)
4. Habib, M., Serebryannikov, A., Caglayan, H., Vandenbosch, E., and Ozbay, E. Collimation, asymmetric beaming, and independent processes in concentric-groove gratings with a single annular hole: Different sides of one phenomenon (Submitted).